

Exact analytical solution of the collapse of self-gravitating Brownian particles and bacterial populations at zero temperature

Pierre-Henri Chavanis¹ and Clément Sire¹

¹*Laboratoire de Physique Théorique (IRSAMC), CNRS and UPS,
Université Paul Sabatier, F-31062 Toulouse, France*

We provide an exact analytical solution of the collapse dynamics of self-gravitating Brownian particles and bacterial populations at zero temperature. These systems are described by the Smoluchowski-Poisson system or Keller-Segel model in which the diffusion term is neglected. As a result, the dynamics is purely deterministic. A cold system undergoes a gravitational collapse leading to a finite time singularity: the central density increases and becomes infinite in a finite time t_{coll} . The evolution continues in the post collapse regime. A Dirac peak emerges, grows and finally captures all the mass in a finite time t_{end} , while the central density excluding the Dirac peak progressively decreases. Close to the collapse time, the pre and post collapse evolutions are self-similar. Interestingly, if one starts from a parabolic density profile, one obtains an exact analytical solution that describes the whole collapse dynamics, from the initial time to the end, and accounts for non self-similar corrections that were neglected in previous works. Our results have possible application in different areas including astrophysics, chemotaxis, colloids and nanoscience.

I. INTRODUCTION

In a series of papers (see [1] for a short review), we have studied a class of mean field drift-diffusion equations of the form

$$\frac{\partial \rho}{\partial t} = \nabla \cdot \left[\frac{1}{\xi} (\nabla p + \rho \nabla \Phi) \right], \quad (1)$$

$$\epsilon \frac{\partial \Phi}{\partial t} = \Delta \Phi - k^2 \Phi - S_d G \rho, \quad (2)$$

where the equation of state $p = p(\rho)$ can take different shapes. These equations, derived in a statistical mechanics context in [2, 3], can be viewed as nonlinear mean field Fokker-Planck (NFP) equations [4] describing a system of Langevin particles in interaction [61]. The first equation (1) can be interpreted as a generalized Smoluchowski equation in which the evolution of the density $\rho(\mathbf{r}, t)$ is due to a competition between a (nonlinear) diffusion and a drift. Contrary to the ordinary Smoluchowski equation [5], the potential $\Phi(\mathbf{r}, t)$ is not fixed but determined by the density itself according to the reaction-diffusion equation (2). Equations (1)-(2) are based on a mean field approximation which is known to be exact for long-range interactions when the number of particles $N \rightarrow +\infty$ [6, 7]. On the other hand, the linear diffusion $\nabla \cdot (D \nabla \rho)$ in the ordinary Smoluchowski equation is replaced by a more general term $\nabla \cdot (\xi^{-1} \nabla p)$ which can lead to anomalous diffusion. The function $p(\mathbf{r}, t) = p[\rho(\mathbf{r}, t)]$ can be interpreted as a barotropic pressure [3]. It can take into account microscopic constraints such as short-range interactions, close packing effects, steric hindrance, non-extensivity, exclusion or inclusion principles... Accordingly, the drift-diffusion equations (1)-(2) are associated with generalized forms of free energy that can be non-Boltzmannian. This leads to a notion of effective generalized thermodynamics (EGT) [3, 4].

The drift-diffusion equations (1)-(2) can be derived heuristically from generalized stochastic processes in physical space of the form

$$\frac{d\mathbf{r}}{dt} = -\frac{1}{\xi} \nabla \Phi + \sqrt{\frac{2p(\rho)}{\xi \rho}} \mathbf{R}(t), \quad (3)$$

where $\Phi(\mathbf{r}, t)$ is a mean field potential determined by Eq. (2) and $\mathbf{R}(t)$ is a Gaussian white noise satisfying $\langle \mathbf{R}(t) \rangle = \mathbf{0}$ and $\langle R_i(t) R_j(t') \rangle = \delta_{ij} \delta(t - t')$ where $i = 1, \dots, d$ label the coordinates of space. The Fokker-Planck equation associated with the generalized Langevin equation (3) is the generalized mean field Smoluchowski equation (1). Note that the strength of the noise can depend on the local density $\rho(\mathbf{r}, t)$ of particles which may lead to anomalous diffusion [8]. The generalized mean field Smoluchowski equation (1) can also be derived from the master equation by assuming that the probabilities of transition explicitly depend on the occupation numbers of the initial and arrival states (see [9] and Sec. 2.11 of [3]). This kinetical interaction principle (KIP) takes into account microscopic constraints such as exclusion or inclusion principles [9].

The model (1)-(2) assumes an overdamped evolution in which the velocity of the particles is directly proportional to the force $-\nabla \Phi$ as in Eq. (3), but more general models taking into account inertial effects can be introduced [3]. They are based on generalized stochastic processes in phase space of the form

$$\frac{d\mathbf{r}}{dt} = \mathbf{v}, \quad (4)$$

$$\frac{d\mathbf{v}}{dt} = -\xi \mathbf{v} - \nabla \Phi + \sqrt{2Df \left[\frac{C(f)}{f} \right]'} \mathbf{R}(t), \quad (5)$$

where the noise depends on the distribution function $f(\mathbf{r}, \mathbf{v}, t)$ of the particles. Here, ξ is a friction coefficient and $C(f)$ is a convex function ($C'' > 0$). This

function determines a generalized entropic functional $S = -\int C(f) d\mathbf{r}d\mathbf{v}$ [3]. The Fokker-Planck equation corresponding to the generalized Langevin equation (5) is the generalized mean field Kramers equation

$$\frac{\partial f}{\partial t} + \mathbf{v} \cdot \frac{\partial f}{\partial \mathbf{r}} - \nabla \Phi \cdot \frac{\partial f}{\partial \mathbf{v}} = \frac{\partial}{\partial \mathbf{v}} \cdot \left[\xi \left(TC''(f) f \frac{\partial f}{\partial \mathbf{v}} + f \mathbf{v} \right) \right], \quad (6)$$

$$\epsilon \frac{\partial \Phi}{\partial t} = \Delta \Phi - k^2 \Phi - S_d G \rho, \quad (7)$$

where we have defined the generalized thermodynamical temperature T through an Einstein-like formula $D = \xi T$ [3]. These equations govern the evolution of the distribution function $f(\mathbf{r}, \mathbf{v}, t)$ in phase space. The generalized Smoluchowski equation (1) can be derived from the generalized Kramers equation (6) in a strong friction limit $\xi \rightarrow +\infty$ by using a Chapman-Enskog expansion [10] or a method of moments [3]. In the strong friction limit, there exists a precise link [3] between the barotropic pressure $p(\rho)$ occurring in the generalized Smoluchowski equation (1) and the function $C(f)$ occurring in the generalized Kramers equation (6). For example, the Boltzmann entropy $S_B = -\int \frac{f}{m} \ln \frac{f}{m} d\mathbf{r}d\mathbf{v}$ (leading to normal diffusion) [5] determines an isothermal equation of state $p(\mathbf{r}, t) = \rho(\mathbf{r}, t) k_B T / m$, where T is the temperature and m the individual mass of the particles. The Tsallis entropy $S_q = -\frac{1}{q-1} \int (f^q - f) d\mathbf{r}d\mathbf{v}$ (leading to anomalous algebraic diffusion) [11] determines a polytropic equation of state $p(\mathbf{r}, t) = K \rho(\mathbf{r}, t)^\gamma$, where K is the polytropic constant and γ the polytropic index. They can be related to T and q as explained in [3]. We can also consider Fermi-Dirac and Bose-Einstein entropies (taking into account exclusion or inclusion constraints) determining fermionic and bosonic equations of state [3]. For example, the equation of state $p(\rho) = -T\sigma_0 \ln(1 - \rho/\sigma_0)$ that takes into account an exclusion constraint in physical space has been studied in [12].

The generalized Smoluchowski equation (1) can also be derived from the damped Euler equations [2, 3]:

$$\frac{\partial \rho}{\partial t} + \nabla \cdot (\rho \mathbf{u}) = 0, \quad (8)$$

$$\frac{\partial \mathbf{u}}{\partial t} + (\mathbf{u} \cdot \nabla) \mathbf{u} = -\frac{1}{\rho} \nabla p - \nabla \Phi - \xi \mathbf{u}. \quad (9)$$

The first equation is the equation of continuity (taking into account the local conservation of mass) and the second equation is the momentum equation. We have assumed that the pressure is isotropic and barotropic, i.e. it is a function of the density $p = p(\rho)$. In the ideal case, it is given by the perfect gas law $p(\mathbf{r}, t) = \rho(\mathbf{r}, t) k_B T / m$. More generally, we allow $p(\rho)$ to be nonlinear so as to take into account microscopic constraints such as short-range interactions and other non ideal effects. In the strong friction limit $\xi \rightarrow +\infty$, we can formally ignore the inertia of the particles in the damped Euler equation leading

to the generalized Darcy law

$$\xi \mathbf{u} \simeq -\frac{1}{\rho} \nabla p - \nabla \Phi. \quad (10)$$

Substituting this relation in the continuity equation (8), we obtain the generalized Smoluchowski equation (1). We note, however, that the damped Euler equations (8)-(9) cannot be directly derived from the stochastic equations (4)-(5) or from the Kramers equation (6) as they rely on a *local thermodynamic equilibrium* (LTE) assumption [2] that is not rigorously justified. By contrast, the generalized Smoluchowski equation (1) can be rigorously derived from the generalized Kramers equation (6) in a strong friction limit $\xi \rightarrow +\infty$ as shown in Refs [3, 10].

We finally note that the generalized mean field Smoluchowski equation (1)-(2) has recently been derived from a kinetic theory [13] that combines the technics used in the theory of systems with long-range interactions and in the theory of liquids (see Appendix C). In this approach, the long-range interactions (leading to the drift) are modeled by using the mean field theory and the short-range interactions (leading to the pressure term) are modeled by using the dynamic density functional theory (DDFT). This new derivation [13] provides an alternative to the kinetic theory based on generalized thermodynamics [3, 4].

The generalized mean field drift-diffusion model (1)-(2) appears in a number of physical situations that we briefly review.

(i) When $\Phi = \Phi_{ext}(\mathbf{r})$ is an external potential and $p = \rho k_B T / m$, we recover the ordinary Smoluchowski equation describing, for example, the sedimentation of colloidal particles in a gravitational field [5]. When $\Phi_{ext} = 0$ and $p = K \rho^\gamma$, we recover the porous medium equation [14]. The porous medium equation with an external potential $\Phi_{ext}(\mathbf{r})$ has been considered by Plastino & Plastino [15] in connection with Tsallis generalized thermodynamics [11].

(ii) When $\epsilon = k = 0$, and for an isothermal equation of state $p = \rho k_B T / m$, we get the Smoluchowski-Poisson system. In the repulsive case $G < 0$, i.e. for the Coulombian interaction, this corresponds to the Debye-Hückel model of electrolytes [16]. The same equations, called the Nernst-Planck equations [17], are also used to study ion transport in biological channels [18, 19] and carrier transport in semiconductors [20]. In the attractive case $G > 0$, i.e. for the gravitational interaction, the Smoluchowski-Poisson system describes a gas of self-gravitating Brownian particles [1]. In that case, G represents the constant of gravity and S_d is the surface of a unit sphere in d dimensions [62].

(iii) When $\epsilon \geq 0$ and $k \geq 0$, we obtain a generalized form of Keller-Segel model [29] describing the chemotaxis of bacterial populations. In that case, ρ denotes the density of bacteria and $c = -\Phi$ the concentration of the secreted chemical. Furthermore, the term $-k^2 \Phi$ takes into account a possible degradation of the chemical, leading to a shielding of the interaction on a scale k^{-1} [12].

(iv) Recently, it has been shown [30] that Eqs. (1)-(2)

with $\epsilon = 0$, $k \geq 0$ and $d = 2$, describe the dynamics of colloids at a fluid interface driven by attractive capillary interactions. In that context, ρ is the particle density, Φ the interfacial deformation and k^{-1} the capillary length whose finiteness leads to a shielding of the interaction. Finally, G is equal to the ratio between the capillary monopole associated to a single particle and the surface tension.

(v) Drift-diffusion equations of the form (1)-(2), or their generalization (see Appendix A), have been proposed to describe phase segregation in model alloys with long-range interactions [31] and aggregation of finite-size particles and directed-assembly processes for nanoscience [32].

(vi) Nonlinear mean field Fokker-Planck equations of the form (1)-(2) and (6)-(2) have also been introduced in two-dimensional (2D) vortex dynamics and stellar dynamics in order to provide a small-scale parametrization of the 2D Euler-Poisson and Vlasov-Poisson systems [33, 34]. They describe the rapid formation of quasi stationary states (QSS) on the coarse-grained scale representing large scale vortices or galaxies [35]. In 2D hydrodynamics, ρ corresponds to the coarse-grained vorticity $\bar{\omega}$ and Φ to the stream function ψ . On the other hand, Eq. (2) reduces to the Poisson equation $-\Delta\psi = \bar{\omega}$. In the case of geophysical flows described by the quasi geostrophic (QG) equations, the Poisson equation is replaced by a screened Poisson equation $-\Delta\psi + \psi/R^2 = \bar{q}$ where R is the Rossby radius and \bar{q} the coarse-grained potential vorticity. In stellar dynamics, \bar{f} is the coarse-grained distribution function, ρ is the density of stars and Φ the gravitational potential.

The numerous analogies between these very different systems, covering all scales of physics (self-gravitating systems, large-scale vortices, biological organisms, electrolytes, colloids, semiconductors, nanotechnology,...) show the importance of studying nonlinear mean field Fokker-Planck equations of the form (1)-(2) and (6)-(2) [63]. Depending on the equation of state $p(\rho, T)$, on the value of the temperature T and on the dimension of space d , the system can either (i) converge towards an equilibrium state, (ii) collapse, or (iii) evaporate. A short description of these different regimes in the case of equations (1)-(2) with $\epsilon = k = 0$ and in the case of isothermal and polytropic equations of state has been given in [1]. It reveals the complexity and the richness of these apparently simple equations.

In this paper, we treat in detail a simple case corresponding to $\epsilon = k = 0$, $G > 0$ (long-range Newtonian interaction) and $p = 0$ (cold system) [64]. In other words, we consider the overdamped dynamics of particles in Newtonian interaction in the zero temperature limit $T = 0$. This system undergoes a gravitational collapse resulting ultimately in the formation of a Dirac peak containing all the mass. As discussed above, this result can have application in other areas such as chemotaxis, colloid dynamics and nanotechnology. Interestingly, if we start from a parabolic density profile,

we can obtain an exact analytical solution of the equations for all times. This solution describes both pre and post collapse regimes. The pre-collapse regime leads to the formation of a finite time singularity: the central density increases like $(t_{coll} - t)^{-1}$ and becomes infinite in a finite time t_{coll} resulting in a singular density profile proportional to $r^{-2d/(d+2)}$. The evolution continues in the post-collapse regime with the formation of a Dirac peak at $r = 0$. The mass contained in the Dirac peak grows like $(t_{coll}/t)^{(d+2)/2}(t - t_{coll})^{d/2}$ while the central density excluding the Dirac peak decreases like $(t - t_{coll})^{-1}(t_{end}/t - 1)$. Finally, in a finite time $t_{end} = ((d+2)/2)t_{coll}$, all the particles are ultimately absorbed by the Dirac peak. In our previous works [36-38], we had only described the self-similar dynamics of the system at $T = 0$ close to the collapse time t_{coll} and for $r \rightarrow 0$. The present analytical solution extends our results to all times $0 \leq t \leq t_{end}$ and all radii $0 \leq r \leq r_{max}(t)$, and describes exact corrections to the self-similar solution. It provides a simple illustration of the Dirac peak formation in the post-collapse regime. These behaviors (pre and post collapse, finite time singularity, growth of a Dirac peak) also arise at $T \neq 0$ (with different exponents) but they are more difficult to investigate analytically [36-39]. Therefore, the present explicit solution can be useful before considering more complicated situations.

II. THE FORMAL SOLUTION OF THE PROBLEM

The Smoluchowski-Poisson (SP) system at $T = 0$ reduces to the form

$$\frac{\partial \rho}{\partial t} = \nabla \cdot \left(\frac{1}{\xi} \rho \nabla \Phi \right), \quad (11)$$

$$\Delta \Phi = S_d G \rho. \quad (12)$$

Equation (11) is equivalent to a continuity equation

$$\frac{\partial \rho}{\partial t} + \nabla \cdot (\rho \mathbf{u}) = 0, \quad (13)$$

with a velocity field

$$\mathbf{u}(\mathbf{r}, t) = -\frac{1}{\xi} \nabla \Phi(\mathbf{r}, t). \quad (14)$$

Introducing a Lagrangian description of motion like in [36], the equation determining the trajectory of a “fluid” particle is

$$\frac{d\mathbf{r}}{dt} = \mathbf{u}(\mathbf{r}, t) = -\frac{1}{\xi} \nabla \Phi(\mathbf{r}, t). \quad (15)$$

It coincides with the equation of motion (3) when the noise is switched off ($T = 0$). In that case, the dynamics is deterministic. If the distribution of particles is initially

spherically symmetric, it will remain spherically symmetric for all times. Using the Gauss theorem, the equation of motion (15) becomes

$$\frac{dr}{dt} = -\frac{1}{\xi} \frac{GM(r, t)}{r^{d-1}}, \quad (16)$$

where

$$M(r, t) = \int_0^r \rho(r_1, t) S_d r_1^{d-1} dr_1, \quad (17)$$

is the mass contained within the sphere of radius r at time t . Conversely,

$$\rho(r, t) = \frac{1}{S_d r^{d-1}} \frac{\partial M}{\partial r}(r, t). \quad (18)$$

Since the equation of motion (16) is a first order differential equation, the particles do not cross each other. Therefore, the conservation of mass implies

$$M(r, t) = M(a, 0), \quad (19)$$

where r is the position at time t of the particle located at $r = a$ at $t = 0$. Equation (16) can therefore be rewritten

$$\frac{dr}{dt} = -\frac{1}{\xi} \frac{GM(a, 0)}{r^{d-1}}, \quad (20)$$

and it is easily integrated into

$$r^d = a^d - \frac{d}{\xi} GM(a, 0)t. \quad (21)$$

Equations (19) and (21) give the general exact solution of the problem [36]. The time at which the particle initially located at $r = a$ reaches the origin $r = 0$ is

$$t_*(a) = \frac{\xi a^d}{dGM(a, 0)}. \quad (22)$$

This time increases with the distance provided that $M(a, 0)/a^d$ is a decreasing function of a (physical case). The opposite situation is treated in Appendix D.

Remark: the gravitational collapse of a cold gas ($T = 0$) initially at rest described by the Euler-Poisson system has been investigated long ago by Hunter [40], Mestel [41] and Penston [42] in astrophysics. In that case, Eq. (20) is replaced by a second order differential equation which can be solved in a parametric form. The collapse of a stellar system which starts from a configuration in which all the stars have zero velocity is initially similar to that of a cold gas at $T = 0$. However, due to fluctuations (finite N effects), the velocity dispersion of the stars increases and orbit crossing occurs [22]. In that case, the mass interior to a given particle changes so that the collapse solution becomes much more complicated. The system undergoes damped oscillations before finally settling on a virialized state as a result of violent relaxation [43]. The simplification obtained by considering self-gravitating Brownian particles in the overdamped limit allows us to obtain a complete and explicit solution of the collapse dynamics for all times since there is no orbit crossing in that case. As we shall see, the system creates a Dirac peak at the origin instead of exhibiting damped oscillations.

III. THE COLLAPSE OF A COLD HOMOGENEOUS SPHERE

Let us first consider the collapse of a homogeneous sphere of mass M and initial radius R . Its initial density is $\rho(a, 0) = dM/(S_d R^d)$ for $a \leq R$ and $\rho(a, 0) = 0$ for $a \geq R$. The corresponding mass profile is

$$M(a, 0) = \frac{M}{R^d} a^d, \quad (23)$$

for $a \leq R$ and $M(a, 0) = M$ for $a \geq R$. According to Eqs. (21) and (23), the position at time t of a particle initially located at $r = a$ is

$$r^d = \left(1 - \frac{dGM}{\xi R^d} t\right) a^d. \quad (24)$$

Therefore, the particles reach $r = 0$ at a time

$$t_* = \frac{\xi R^d}{dGM}, \quad (25)$$

whatever their initial position a . This leads to a complete collapse of the system (Dirac peak) at a time $t = t_*$. According to Eqs. (19), (23) and (24), the mass profile at time t is

$$M(r, t) = \frac{M}{R^d} \frac{r^d}{1 - \frac{t}{t_*}}. \quad (26)$$

The sphere of particles remains spatially homogeneous with a radius decreasing in time like

$$R(t) = R \left(1 - \frac{t}{t_*}\right)^{1/d}. \quad (27)$$

The density increases with time like

$$\rho(t) = \frac{\rho(0)}{1 - \frac{t}{t_*}}. \quad (28)$$

This result can be directly obtained from Eqs. (11)-(12) using the fact that the density is spatially homogeneous. Indeed, using the Poisson equation (12), Eq. (11) becomes

$$\frac{d\rho}{dt} = \frac{S_d G}{\xi} \rho^2, \quad (29)$$

which leads to Eq. (28) after integration.

Remark: in the context of the Euler-Poisson system at $T = 0$, the free-fall time of a homogeneous sphere is $t_{ff} = (3\pi/32G\rho_0)^{1/2}$ (in $d = 3$) [40]. This is of the order of the dynamical time $t_{dyn} = (3\pi/16G\rho_0)^{1/2}$ [22]. For the Smoluchowski-Poisson system at $T = 0$, the collapse time (25) of a homogeneous sphere can be written $t_* = \xi/S_d \rho_0 G$. It is of the order ξt_{dyn}^2 .

IV. THE PRE-COLLAPSE OF A PARABOLIC PROFILE

A. The exact solution

We now consider an initial mass profile of the form

$$M(a, 0) = A(a^d - Ba^{d+2}), \quad (30)$$

where A and B are two positive constants. Using Eq. (18), we find that the corresponding density profile is parabolic

$$\rho(a, 0) = \frac{dA}{S_d} \left(1 - \frac{d+2}{d} Ba^2 \right). \quad (31)$$

These expressions are valid for $a \leq R$ where R is the radius at which the density vanishes. The constant B is related to the radius R of the initial configuration by

$$B = \frac{d}{(d+2)R^2}. \quad (32)$$

On the other hand, the constant A is related to the total mass M of the system, and to its radius R , by

$$A = \frac{d+2}{2} \frac{M}{R^d}. \quad (33)$$

According to Eqs. (21) and (30), the position at time t of a particle initially located at $r = a$ is

$$r^d = a^d - \frac{d}{\xi} GAa^d(1 - Ba^2)t. \quad (34)$$

The time at which the particle initially located at $r = a > 0$ reaches the origin $r = 0$ is

$$t_*(a) = \frac{\xi}{dGA(1 - Ba^2)}. \quad (35)$$

In particular, the time at which the last particle, i.e. the one initially located at $a = R$, reaches the origin is

$$t_{end} = \frac{(d+2)\xi}{2dGA} = \frac{\xi R^d}{dGM}. \quad (36)$$

This is the final time since, at that time, all the particles have collapsed at the origin. The density profile is a Dirac peak $\rho = M\delta(\mathbf{r})$ containing all the mass and there is no further evolution. As may appear surprising at first sight, the time at which the first particle, i.e. the one initially located at $a = 0^+$, reaches the origin is *finite*:

$$t_{coll} = \frac{\xi}{dGA} = \frac{2\xi R^d}{d(d+2)GM}. \quad (37)$$

This is the time at which the density profile becomes singular at the origin, since an infinitesimal number of particles has reached $r = 0$. This corresponds to a finite

time singularity in which the central density diverges. We note that

$$t_{end} = \frac{d+2}{2} t_{coll}. \quad (38)$$

Combining the foregoing equations, the conservation of mass (19) and the equation of motion (21) can be written

$$M(r, t) = \frac{\xi}{dGt_{coll}} a^d (1 - Ba^2), \quad (39)$$

$$r^d = \frac{1}{t_{coll}} (t_{coll} - t) a^d + B \frac{t}{t_{coll}} a^{d+2}. \quad (40)$$

These equations, parameterized by a , completely determine the evolution of the mass profile for all times. However, in order to exhibit the self-similar structure of the solution close to t_{coll} (see Sec. IV B), it is convenient to define

$$y = \frac{1}{t_{coll}} \frac{a^d}{(t_{coll} - t)^{d/2}}, \quad (41)$$

and

$$C = B t_{coll}^{(d+2)/d}, \quad (42)$$

in which case, Eqs. (39) and (40) can be rewritten

$$M(r, t) = \frac{\xi}{dG} (t_{coll} - t)^{d/2} y \left(1 - C \frac{t_{coll} - t}{t_{coll}} y^{2/d} \right), \quad (43)$$

$$x^d = y + C \frac{t}{t_{coll}} y^{(d+2)/d}, \quad (44)$$

$$x = \frac{r}{(t_{coll} - t)^{(d+2)/2d}}, \quad (45)$$

where x is the appropriate scaling variable and y is just a dummy variable. Using Eqs. (18), (43) and (44), the corresponding density profile is

$$\rho(r, t) = \frac{\xi}{S_d G} \frac{1}{t_{coll} - t} \left[1 - \frac{C}{t_{coll}} (t_{coll} - t) \frac{2+d}{d} y^{2/d} \right] \times \frac{1}{\frac{d+2}{d} C \frac{t}{t_{coll}} y^{2/d} + 1}. \quad (46)$$

The central density behaves like

$$\rho(0, t) = \frac{\xi}{S_d G} \frac{1}{t_{coll} - t}, \quad (47)$$

and it diverges at $t = t_{coll}$. Finally, according to Eq. (40), the position at time t of the last particle, i.e. the one located at $a = R$ at time $t = 0$, is

$$r_{max}(t)^d = \frac{1}{t_{coll}} (t_{coll} - t) R^d + B \frac{t}{t_{coll}} R^{d+2}. \quad (48)$$

We can check that $\rho(r_{max}, t) = 0$. Let us now consider particular limits of these equations.

For $t \rightarrow 0$, we obtain after some calculations

$$\rho(r, t) \simeq \rho(r, 0) + \frac{\xi}{S_d G t_{coll}} \frac{t}{t_{coll}} \left[1 - B \frac{2(d+1)(d+2)}{d^2} r^2 + B^2 \frac{(d+2)(d+4)}{d^2} r^4 \right]. \quad (49)$$

The corresponding mass profile is

$$M(r, t) \simeq M(r, 0) + \frac{\xi}{G t_{coll}} \frac{t}{t_{coll}} \left[\frac{r^d}{d} - B \frac{2(d+1)}{d^2} r^{d+2} + B^2 \frac{d+2}{d^2} r^{d+4} \right]. \quad (50)$$

This is valid for $r \leq r_{max}(t)$ with

$$r_{max}(t) \simeq R \left[1 - \frac{2}{d(d+2)} \frac{t}{t_{coll}} \right]. \quad (51)$$

For $t \rightarrow 0$, the central density behaves like

$$\rho(0, t) \simeq \frac{\xi}{S_d G t_{coll}} \left(1 + \frac{t}{t_{coll}} \right). \quad (52)$$

Taking $t = t_{coll}$ in Eqs. (43)-(45), and using $x^d = C y^{(d+2)/d}$, we obtain the exact profiles

$$M(r, t_{coll}) = \frac{\xi}{dG} \frac{1}{C^{d/(d+2)}} r^{d^2/(d+2)} \times \left[1 - \frac{C^{d/(d+2)}}{t_{coll}} r^{2d/(d+2)} \right], \quad (53)$$

$$\rho(r, t_{coll}) = \frac{\xi}{S_d G} \frac{d}{d+2} \frac{1}{C^{d/(d+2)}} \frac{1}{r^{2d/(d+2)}} \times \left[1 - \frac{d+2}{d} \frac{C^{d/(d+2)}}{t_{coll}} r^{2d/(d+2)} \right]. \quad (54)$$

According to Eqs. (48) and (42), the position at time t_{coll} of the last particle is

$$r_{max} = \frac{C^{1/d}}{t_{coll}^{(d+2)/d^2}} R^{(d+2)/d}. \quad (55)$$

We can check that $M(r_{max}, t_{coll}) = M$. More precisely, using Eqs. (53) and (54), we find that

$$M(r, t_{coll}) \simeq M \left[1 - \frac{d^3}{2(d+2)} \left(\frac{r_{max} - r}{r_{max}} \right)^2 \right], \quad (56)$$

$$\rho(r, t_{coll}) \simeq \frac{d^2 M}{S_d R^d} \left(1 - \frac{r}{r_{max}} \right), \quad (57)$$

for $r \rightarrow r_{max}$. The behavior of $M(r, t_{coll})$ and $\rho(r, t_{coll})$ for $r \rightarrow 0$ is given in the following section.

B. Self-similar solution for $t \rightarrow t_{coll}$ and $r \rightarrow 0$

For $t \rightarrow t_{coll}$ and $r \rightarrow 0$, Eqs. (43)-(45) reduce to the form

$$M(r, t) = \frac{\xi}{dG} (t_{coll} - t)^{d/2} y, \quad (58)$$

$$x^d = y + C y^{(d+2)/d}, \quad (59)$$

$$x = \frac{r}{(t_{coll} - t)^{(d+2)/2d}}, \quad (60)$$

showing that the evolution becomes self-similar as we approach the collapse time. The corresponding density profile is

$$\rho(r, t) = \frac{\xi}{S_d G} \frac{1}{t_{coll} - t} \frac{1}{1 + \frac{d+2}{d} C y^{2/d}}. \quad (61)$$

The central density increases like

$$\rho(0, t) = \frac{\xi}{S_d G} \frac{1}{t_{coll} - t}, \quad (62)$$

and diverges at the collapse time. In parallel, the typical core radius

$$r_0(t) \sim (t_{coll} - t)^{(d+2)/2d}. \quad (63)$$

appearing in Eq. (60) decreases and tends to zero at $t = t_{coll}$. Comparing Eq. (63) with Eq. (62), we find that the core radius is related to the central density $\rho_0(t) = \rho(0, t)$ by the relation

$$\rho_0 r_0^\alpha \sim 1, \quad (64)$$

involving the scaling exponent

$$\alpha = \frac{2d}{d+2}. \quad (65)$$

Note also that the mass within the core radius is

$$M(r_0(t), t) \sim \rho_0(t) r_0^d(t) \sim (t_{coll} - t)^{d/2}, \quad (66)$$

and it tends to zero as $t \rightarrow t_{coll}$. Therefore, there is no Dirac peak in the pre-collapse regime.

For $t = t_{coll}$ and $r \rightarrow 0$, Eq. (59) reduce to $x^d = C y^{(d+2)/d}$ and we obtain the power-law profiles

$$M(r, t_{coll}) = \frac{\xi}{dG} \frac{1}{C^{d/(d+2)}} r^{d^2/(d+2)}, \quad (67)$$

$$\rho(r, t_{coll}) = \frac{\xi}{S_d G} \frac{d}{d+2} \frac{1}{C^{d/(d+2)}} \frac{1}{r^{2d/(d+2)}}. \quad (68)$$

They can also be derived from Eqs. (53) and (54) for $r \rightarrow 0$. This shows that the system develops a finite time singularity: the density profile diverges at the origin and scales like $r^{-2d/(d+2)}$. By contrast, the mass $M(r, t_{coll})$ tends to zero at the origin. This means that only an *infinitesimal* number of particles has reached the origin at $t = t_{coll}$, leading to infinite central density but zero central mass.

C. The half central density radius

Using Eq. (46), the radius $r_*(t)$ corresponding to half the central density, i.e. such that $\rho(r_*(t), t) = \rho(0, t)/2$, is

$$r_*(t) = \left(\frac{d}{d+2} \frac{1}{C} \right)^{1/2} \frac{(t_{coll} - t)^{(d+2)/2d}}{\left(2 - \frac{t}{t_{coll}} \right)^{(d+2)/2d}} \times \left(2 - \frac{2}{d+2} \frac{t}{t_{coll}} \right)^{1/d}. \quad (69)$$

For $t = 0$, we obtain

$$r_*(0) = \frac{R}{\sqrt{2}}, \quad (70)$$

a result that can be directly obtained from Eq. (31). For $t \rightarrow 0$, we find that

$$r_*(t) \simeq \frac{R}{\sqrt{2}} \left[1 - \frac{d^2 + 4d + 8}{4d(d+2)} \frac{t}{t_{coll}} \right]. \quad (71)$$

For $t = t_{coll}$, Eq. (69) gives $r_* = 0$. In the self-similar regime $t \rightarrow t_{coll}$, we find that

$$r_*(t) = \left(\frac{d}{d+2} \frac{1}{C} \right)^{1/2} \left[\frac{2(d+1)}{d+2} \right]^{1/d} (t_{coll} - t)^{(d+2)/2d}. \quad (72)$$

In the self-similar regime, the half central density radius $r_*(t)$ behaves like the typical core radius $r_0(t)$, see Eq. (63). The mass within the sphere of radius r_* evolves with time like

$$M(r_*(t), t) \sim \rho_0(t) r_*(t)^d \sim \frac{2 - \frac{2}{d+2} \frac{t}{t_{coll}}}{\left(2 - \frac{t}{t_{coll}} \right)^{(d+2)/2}} (t_{coll} - t)^{d/2}. \quad (73)$$

In the self-similar regime, we find that $M(r_*(t), t)$ tends to zero like $\sim (t_{coll} - t)^{d/2} \sim M(r_0(t), t)$.

D. More explicit solutions for $d = 2$

In $d = 2$, Eq. (44) can be solved explicitly to obtain $y(x, t)$. Therefore, the exact solution can be written

$$M(r, t) = \frac{\xi}{2G} (t_{coll} - t) y \left(1 - C \frac{t_{coll} - t}{t_{coll}} y \right), \quad (74)$$

$$\rho(r, t) = \frac{\xi}{2\pi G} \frac{1}{t_{coll} - t} \left[1 - \frac{2C}{t_{coll}} (t_{coll} - t) y \right] \frac{1}{\frac{2Ct}{t_{coll}} y + 1}, \quad (75)$$

$$y = \frac{-1 + \sqrt{1 + 4C \frac{t}{t_{coll}} x^2}}{\frac{2Ct}{t_{coll}}}, \quad (76)$$

$$x = \frac{r}{t_{coll} - t}. \quad (77)$$

For $t \rightarrow t_{coll}$ and $r \rightarrow 0$, the self-similar solution can be written

$$M(r, t) = \frac{\xi}{2G} (t_{coll} - t) y, \quad (78)$$

$$\rho(r, t) = \frac{\xi}{2\pi G} \frac{1}{t_{coll} - t} \frac{1}{2Cy + 1}, \quad (79)$$

$$y = \frac{-1 + \sqrt{1 + 4Cx^2}}{2C}, \quad (80)$$

$$x = \frac{r}{t_{coll} - t}. \quad (81)$$

V. THE POST-COLLAPSE REGIME

The previous solution shows that the system forms a finite time singularity: the central density becomes infinite in a finite time $t = t_{coll}$. However, the mass contained within a sphere of radius ϵ tends to zero as $\epsilon \rightarrow 0$. This is due to the fact that only an *infinitesimal* number of particles has reached $r = 0$ at $t = t_{coll}$ leading to infinite central density but zero central mass. This cannot be the final equilibrium state of the system since statistical mechanics predicts that the equilibrium state of a self-gravitating gas in the canonical ensemble is a Dirac peak containing all the particles (this is the configuration that makes the free energy tend to $-\infty$ due to the divergence of energy) [44, 45]. This is true at any temperature. For a self-gravitating Brownian gas a $T = 0$, we have previously established that the Dirac peak $\rho(\mathbf{r}) = M\delta(\mathbf{r})$ forms at a time t_{end} given by Eq. (36). Therefore, the evolution continues in the post collapse regime $t_{coll} \leq t \leq t_{end}$ where a Dirac peak grows and accretes progressively all the surrounding particles. The exact description of this process for $T = 0$ is the object of the present section.

A. The exact solution

For $t \geq t_{coll}$, the equation of motion (21) can be written

$$r^d = a^d - \frac{d}{\xi} GM(a, t_{coll})(t - t_{coll}), \quad (82)$$

where $M(a, t_{coll})$ is the mass profile at time $t = t_{coll}$. Using Eq. (53), we obtain

$$r^d = a^d - \frac{1}{C^{d/(d+2)}} a^{d^2/(d+2)} \times \left[1 - \frac{C^{d/(d+2)}}{t_{coll}} a^{2d/(d+2)} \right] (t - t_{coll}). \quad (83)$$

At $t = t_{coll} + \Delta t$, the mass contained within the sphere of radius a_* at $t = t_{coll}$ has reached $r = 0$. From Eq. (83), we get

$$a_*^{2d/(d+2)} = \frac{\Delta t}{C^{d/(d+2)}} \frac{1}{1 + \frac{\Delta t}{t_{coll}}}. \quad (84)$$

This leads to the formation of a Dirac peak of mass $M_D(t) = M(a_*, t_{coll})$. Substituting Eq. (84) in Eq. (53), we obtain

$$M_D(t) = \frac{\xi}{dG} \frac{1}{C^{d/2}} \left(\frac{t_{coll}}{t} \right)^{(d+2)/2} (t - t_{coll})^{d/2}. \quad (85)$$

We can check that $M_D(t_{end}) = M$ so that all the mass has been absorbed in the Dirac peak at $t = t_{end}$. More precisely, we find that

$$M_D(t) \simeq M \left[1 - \frac{d+2}{2d} \left(1 - \frac{t}{t_{end}} \right)^2 \right], \quad (86)$$

for $t \rightarrow t_{end}$. It is relevant to write the conservation of mass (19) in the form

$$M_{tot}(r, t) \equiv M_D(t) + M(r, t) = M(a, t_{coll}), \quad (87)$$

where $M_D(t)$ is the mass contained in the Dirac peak and $M(r, t)$ is the mass exterior to the Dirac. Similarly, we write the density profile as

$$\rho_{tot}(\mathbf{r}, t) = M_D(t)\delta(\mathbf{r}) + \rho(\mathbf{r}, t). \quad (88)$$

The regular part of the profile $\rho(\mathbf{r}, t)$ is the residual density defined as the density after the central peak has been subtracted. Using Eq. (53), the evolution of the mass profile in the post-collapse regime is given by

$$M_D(t) + M(r, t) = \frac{\xi}{dG} \frac{1}{C^{d/(d+2)}} a^{d^2/(d+2)} \times \left[1 - \frac{C^{d/(d+2)}}{t_{coll}} a^{2d/(d+2)} \right], \quad (89)$$

$$r^d = a^d - \frac{1}{C^{d/(d+2)}} a^{d^2/(d+2)} \times \left[1 - \frac{C^{d/(d+2)}}{t_{coll}} a^{2d/(d+2)} \right] (t - t_{coll}). \quad (90)$$

These equations completely determine the evolution of the mass profile in the post-collapse regime. In order to exhibit the self-similar structure of the solution close to t_{coll} (see Sec. VB), it is convenient to define

$$y = \frac{1}{C^{d/(d+2)}} \frac{a^{d^2/(d+2)}}{(t - t_{coll})^{d/2}}, \quad (91)$$

in which case, Eqs. (89) and (90) can be rewritten

$$M_D(t) + M(r, t) = \frac{\xi}{dG} (t - t_{coll})^{d/2} \times y \left(1 - C \frac{t - t_{coll}}{t_{coll}} y^{2/d} \right), \quad (92)$$

$$x^d = C \frac{t}{t_{coll}} y^{(d+2)/d} - y, \quad (93)$$

$$x = \frac{r}{(t - t_{coll})^{(d+2)/2d}}. \quad (94)$$

Note the similarities and the differences with the pre-collapse solution (43)-(45). If we subtract the contribution of the Dirac peak, using Eq. (85), we obtain

$$M(r, t) = \frac{\xi}{dG} (t - t_{coll})^{d/2} \times \left[y \left(1 - C \frac{t - t_{coll}}{t_{coll}} y^{2/d} \right) - \frac{1}{C^{d/2}} \left(\frac{t_{coll}}{t} \right)^{(d+2)/2} \right], \quad (95)$$

$$x^d = C \frac{t}{t_{coll}} y^{(d+2)/d} - y, \quad (96)$$

$$x = \frac{r}{(t - t_{coll})^{(d+2)/2d}}. \quad (97)$$

Using Eqs. (18), (95) and (96), the corresponding density profile is

$$\rho(r, t) = \frac{\xi}{S_d G} \frac{1}{t - t_{coll}} \left[1 - \frac{C}{t_{coll}} (t - t_{coll}) \frac{2+d}{d} y^{2/d} \right] \times \frac{1}{\frac{d+2}{d} C \frac{t}{t_{coll}} y^{2/d} - 1}. \quad (98)$$

According to Eqs. (98), (96) and (97), the central residual density decreases with time like

$$\rho(0, t) = \frac{\xi}{S_d G} \frac{1}{t - t_{coll}} \left(\frac{t_{end}}{t} - 1 \right). \quad (99)$$

Let us now consider particular limits of these equations.

For $t = t_{coll}$, we recover the results (53)-(57). For $t = t_{end}$, using Eq. (48), we can check that $r_{max}(t_{end}) = 0$. More precisely, for $t \rightarrow t_{end}$, we obtain after some calculations

$$\rho(r, t) \simeq \frac{2\xi}{dS_d G} \frac{1}{t_{coll}} \left[\frac{t_{end} - t}{t_{end}} - C^{d/2} \left(\frac{d+2}{d} \right)^{d/2} \frac{r^d}{t_{coll}^{(d+2)/2}} \right]. \quad (100)$$

The corresponding mass profile is

$$M(r, t) \simeq \frac{2\xi r^d}{d^2 G t_{coll}} \left[\frac{t_{end} - t}{t_{end}} - \left(\frac{d+2}{d} \right)^{d/2} \frac{r^d}{2 t_{coll}^{(d+2)/2}} \right]. \quad (101)$$

This is valid for $r \leq r_{max}(t)$ with

$$r_{max} \simeq \left(\frac{t_{end} - t}{t_{end}} \right)^{1/d} R. \quad (102)$$

The total mass outside the Dirac is $M(t) = M(r_{max}, t)$. Using Eqs. (101) and (102), we obtain

$$M(t) \simeq M \frac{d+2}{2d} \left(\frac{t_{end} - t}{t_{end}} \right)^2. \quad (103)$$

Comparing with Eq. (86), we check that $M_D(t) + M(t) = M$, as it should. On the other hand, for $t \rightarrow t_{end}$, the central density (99) decreases like

$$\rho(0, t) \simeq \frac{2\xi}{dS_d G} \frac{1}{t_{coll}} \left(1 - \frac{t}{t_{end}} \right), \quad (104)$$

in agreement with Eq. (100).

B. Self-similar solution for $t \rightarrow t_{coll}$ and $r \rightarrow 0$

As the Dirac peak grows in the post-collapse regime, the central residual density decreases. Soon after $t = t_{coll}$, the residual density profile $\rho(r, t)$ follows a post-collapse self-similar evolution, reverse to the pre-collapse self-similar evolution, during which the central residual density $\rho(0, t)$ decreases while the core radius $r_0(t)$ increases. This is the object of the present subsection.

For $t \rightarrow t_{coll}$, the mass of the Dirac grows like

$$M_D(t) = \frac{\xi}{dG} \frac{1}{C^{d/2}} (t - t_{coll})^{d/2}. \quad (105)$$

Furthermore, for $t \rightarrow t_{coll}$ and $r \rightarrow 0$, Eqs. (95)-(97) reduce to the form

$$M(r, t) = \frac{\xi}{dG} (t - t_{coll})^{d/2} \left(y - \frac{1}{C^{d/2}} \right), \quad (106)$$

$$x^d = C y^{(d+2)/d} - y, \quad (107)$$

$$x = \frac{r}{(t - t_{coll})^{(d+2)/2d}}, \quad (108)$$

showing that the evolution is self-similar just after the collapse time. The corresponding density profile is

$$\rho(r, t) = \frac{\xi}{S_d G} \frac{1}{t - t_{coll}} \frac{1}{\frac{d+2}{d} C y^{2/d} - 1}. \quad (109)$$

The central residual density behaves like

$$\rho(0, t) = \frac{d\xi}{2S_d G} \frac{1}{t - t_{coll}}. \quad (110)$$

Therefore, the central residual density decreases as more and more mass is absorbed in the Dirac peak. In parallel, the typical core radius

$$r_0(t) \sim (t - t_{coll})^{(d+2)/2d}, \quad (111)$$

appearing in Eq. (108) increases. Comparing Eq. (111) with Eq. (110), we find that the core radius is related to the central density $\rho_0(t) = \rho(0, t)$ by the relation

$$\rho_0 r_0^\alpha \sim 1, \quad (112)$$

involving the scaling exponent

$$\alpha = \frac{2d}{d+2}, \quad (113)$$

the same as in the pre-collapse regime. The mass within the core radius is

$$M(r_0(t), t) \sim \rho_0(t) r_0^d(t) \sim (t - t_{coll})^{d/2}, \quad (114)$$

and it increases with time. Note that the mass (105) contained in the Dirac peak has a similar scaling.

C. The half central density radius

In the self-similar regime, the core radius $r_0(t)$ increases with time indicating that the residual density profile expands as the central density decreases. However, since the system size $r_{max}(t)$ decreases to zero for $t = t_{end}$, the expansion of the density profile cannot be valid for all times. In fact, the core radius $r_0(t)$ makes sense only during the self-similar regime. To study the evolution of the residual density profile in a more general setting, we introduce the half central density radius $r_*(t)$.

Using Eq. (98), the radius $r_*(t)$ corresponding to half the central density, i.e. such that $\rho(r_*(t), t) = \rho(0, t)/2$, is

$$r_*(t) = \left(\frac{t_{coll}}{C} \frac{d}{d+2} \right)^{1/2} \frac{\left(\frac{1}{2} + \frac{2+d}{4} \frac{t_{coll}}{t} \right)^{1/2}}{\left(\frac{d-2}{4} t_{coll} + \frac{t}{2} \right)^{(d+2)/2d}} \times \left(\frac{1}{2} t_{coll} - \frac{t}{d+2} \right)^{1/d} (t - t_{coll})^{(d+2)/2d}. \quad (115)$$

For $t = t_{coll}$, this formula gives $r_* = 0$. In the self-similar regime $t \rightarrow t_{coll}$, we have

$$r_*(t) = \frac{\left(\frac{4+d}{d+2} \right)^{1/2} \left(\frac{2}{d+2} \right)^{1/d}}{C^{1/2}} (t - t_{coll})^{(d+2)/2d}. \quad (116)$$

For $t \rightarrow t_{end}$, we obtain

$$r_*^d(t) \simeq \frac{1}{C^{d/2}} \left(\frac{d}{d+2} \right)^{d/2} \frac{t_{end} - t}{2t_{end}} t_{coll}^{(d+2)/2}, \quad (117)$$

a result that can also be directly obtained from Eq. (100). In the self-similar regime, we find that $r_*(t) \propto (t - t_{coll})^{(d+2)/2d}$ behaves like $r_0(t)$ so that the density profile spreads. Then, $r_*(t)$ decreases and behaves like $r_* \propto (t_{end} - t)^{1/d}$ for $t \rightarrow t_{end}$ so that the density profile

shrinks. The mass within the sphere of radius r_* evolves with time like

$$M(r_*(t), t) \sim \rho_0(t) r_*(t)^d \sim \frac{(t_{end} - t)^2}{t} \frac{\left(\frac{1}{2} + \frac{2+d}{4} \frac{t_{coll}}{t}\right)^{d/2}}{\left(\frac{d-2}{4} t_{coll} + \frac{t}{2}\right)^{(d+2)/2}} (t - t_{coll})^{d/2}. \quad (118)$$

In the self-similar regime, we find that $M(r_*(t), t)$ increases like $\sim (t - t_{coll})^{d/2} \sim M(r_0(t), t)$. Then, $M(r_*(t), t)$ decreases and behaves like $M(r_*(t), t) \sim (t_{end} - t)^2$ for $t \rightarrow t_{end}$.

D. More explicit solutions for $d = 2$

In $d = 2$, Eq. (96) can be solved explicitly to obtain $y(x, t)$. Therefore, the exact solution can be written

$$M(r, t) = \frac{\xi}{2G} (t - t_{coll}) \times \left[y \left(1 - C \frac{t - t_{coll}}{t_{coll}} y \right) - \frac{1}{C} \left(\frac{t_{coll}}{t} \right)^2 \right], \quad (119)$$

$$\rho(r, t) = \frac{\xi}{2\pi G} \frac{1}{t - t_{coll}} \left[1 - \frac{2C}{t_{coll}} (t - t_{coll}) y \right] \times \frac{1}{2C \frac{t}{t_{coll}} y - 1}, \quad (120)$$

$$y = \frac{1 + \sqrt{1 + 4C \frac{t}{t_{coll}} x^2}}{\frac{2Ct}{t_{coll}}}, \quad (121)$$

$$x = \frac{r}{t - t_{coll}}. \quad (122)$$

For $t \rightarrow t_{coll}$ and $r \rightarrow 0$, the self-similar solution can be written

$$M(r, t) = \frac{\xi}{2G} (t - t_{coll}) \left(y - \frac{1}{C} \right), \quad (123)$$

$$\rho(r, t) = \frac{\xi}{2\pi G} \frac{1}{t - t_{coll}} \frac{1}{2Cy - 1}, \quad (124)$$

$$y = \frac{1 + \sqrt{1 + 4Cx^2}}{2C}, \quad (125)$$

$$x = \frac{r}{t - t_{coll}}. \quad (126)$$

VI. ILLUSTRATION OF THE RESULTS

We shall now illustrate the previous analytical results by plotting some relevant quantities. For simplicity, we consider a two-dimensional system ($d = 2$) [65] and choose a system of units such that $M = R = t_{coll} = 1$. With these conventions, we have $A = 2$, $B = 1/2$ and $C = 1/2$. On the other hand, $\xi/G = 4$ and $S_2 = 2\pi$.

The initial density profile ($t = 0$) is the parabole

$$\rho(r, 0) = \frac{2}{\pi} (1 - r^2). \quad (127)$$

The finite time singularity occurs at $t = t_{coll} = 1$ and the Dirac peak containing the whole mass is formed at $t = t_{end} = 2$. The size of the system, i.e. the radius at which the density vanishes, decreases like

$$r_{max}(t) = \left(1 - \frac{t}{2} \right)^{1/2}. \quad (128)$$

The exact density profile for $0 \leq t \leq t_{coll} = 1$ (pre-collapse) is

$$\rho(r, t) = \frac{1}{1-t} \frac{2}{\pi} \frac{1}{\sqrt{1 + 2tx^2}}, \times \left[1 - \frac{1-t}{t} \left(\sqrt{1 + 2tx^2} - 1 \right) \right], \quad (129)$$

$$x = \frac{r}{1-t}. \quad (130)$$

For short times $t \rightarrow 0$, it is approximately given by

$$\rho(r, t) \simeq \rho(r, 0) + \frac{2}{\pi} \left(1 - 3r^2 + \frac{3}{2}r^4 \right) t, \quad (131)$$

for $r \leq r_{max} \simeq 1 - t/4$ (see Fig. 1). For $0 \leq t \leq t_{coll} = 1$, the central density increases like (see Fig. 2):

$$\rho(0, t) = \frac{2}{\pi} \frac{1}{1-t}. \quad (132)$$

For $t \rightarrow t_{coll} = 1$ and $r \rightarrow 0$, the density distribution takes the self-similar form

$$\rho_{ss}(r, t) = \frac{1}{1-t} f\left(\frac{r}{1-t}\right), \quad (133)$$

with the invariant profile

$$f(x) = \frac{2}{\pi} \frac{1}{\sqrt{1 + 2x^2}}. \quad (134)$$

The central density corresponding to the self-similar solution (133) is

$$\rho_{ss}(0, t) = \frac{2}{\pi} \frac{1}{1-t}, \quad (135)$$

and it exactly coincides with Eq. (132). The singular profile corresponding to the self-similar solution (133) at $t = t_{coll} = 1$ is

$$\rho_{ss}(r, t_{coll}) = \frac{\sqrt{2}}{\pi r}. \quad (136)$$

The exact density profile at $t = t_{coll} = 1$ is

$$\rho(r, t_{coll}) = \frac{\sqrt{2}}{\pi} \left(\frac{1}{r} - \sqrt{2} \right). \quad (137)$$

for $r \leq r_{max} = 1/\sqrt{2}$. The exact density profile is plotted in Fig. 3 using self-similar variables. This representation illustrates the fact that the solution becomes self-similar for $t \rightarrow t_{coll} = 1$; indeed the curves tends to the invariant profile (134). The exact density profile is also plotted in Fig. 4 in logarithmic variables. This representation illustrates the fact that the density displays a finite time singularity at $t \rightarrow t_{coll} = 1$ and that, approaching the singularity, the profile becomes self-similar. For sufficiently small $t_{coll} - t$, the tail of the profile (for $r_0(t) \ll r \ll r_{max}(t)$) is well-approximated by the pure power law (136) but if we want to describe the distribution up to $r_{max}(t) \sim 1/\sqrt{2}$, we must use the truncated power law (137).

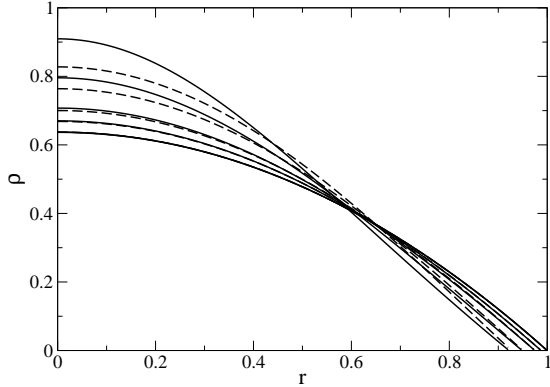


FIG. 1: Evolution of the density profile $\rho(r, t)$ for small times. We have taken $t = 0, 0.05, 0.1, 0.2, 0.3$. The full lines correspond to the exact profile (129) and the dashed lines to the approximation (131) valid for $t \ll 1$.

For $t_{coll} = 1 \leq t \leq t_{end} = 2$ (post-collapse), the mass contained in the Dirac peak grows like (see Fig. 5):

$$M_D(t) = \frac{4}{t^2}(t-1). \quad (138)$$

The exact residual density profile is

$$\rho(r, t) = \frac{1}{t-1} \frac{2}{\pi} \frac{1}{\sqrt{1+2tx^2}}, \quad (139)$$

$$\times \left[1 - \frac{t-1}{t} \left(1 + \sqrt{1+2tx^2} \right) \right],$$

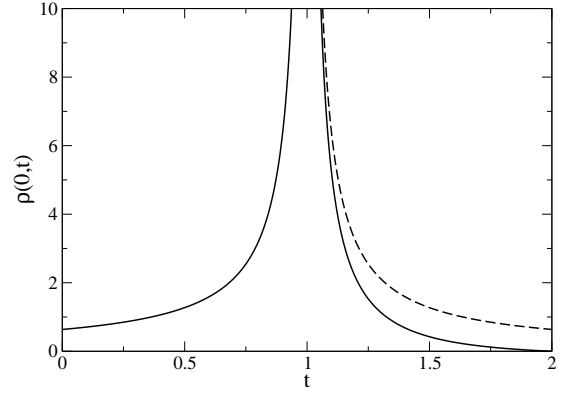


FIG. 2: Evolution of the central density in the pre and post collapse regimes. The dashed line corresponds to the self-similar solution valid for $t \rightarrow t_{coll} = 1$.

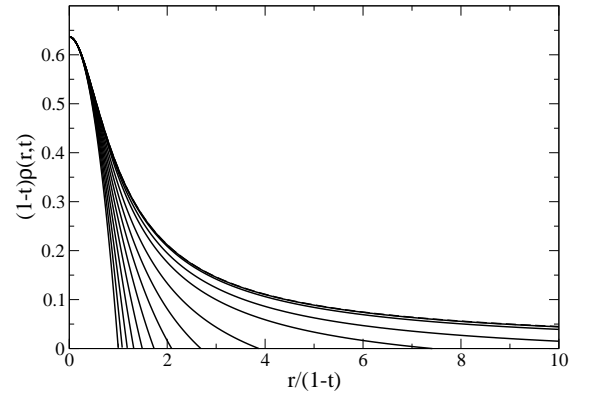


FIG. 3: Evolution of the density profile $\rho(r, t)$ using self-similar variables. We have taken $t = 0, 0.1, 0.2, 0.3, 0.4, 0.5, 0.6, 0.7, 0.8, 0.9, 0.95, 0.99, 0.999$. The full lines correspond to the exact profile (129)-(130). They tend to the invariant profile (134) represented by a dashed line (hardly visible).

$$x = \frac{r}{t-1}. \quad (140)$$

For $t \rightarrow t_{end} = 2$, it is approximately given by

$$\rho(r, t) = \frac{2}{\pi} \left(\frac{2-t}{2} - r^2 \right), \quad (141)$$

for $r \leq r_{max} \simeq [(2-t)/2]^{1/2}$ (see Fig. 6). For $t_{coll} = 1 \leq t \leq t_{end} = 2$, the central density decreases like (see Fig. 2):

$$\rho(0, t) = \frac{2}{\pi} \frac{1}{t-1} \left(\frac{2}{t} - 1 \right). \quad (142)$$

For $t \rightarrow t_{coll} = 1^+$ and $r \rightarrow 0$, the residual density distribution takes the self-similar form

$$\rho_{ss}(r, t) = \frac{1}{t-1} f \left(\frac{r}{t-1} \right), \quad (143)$$

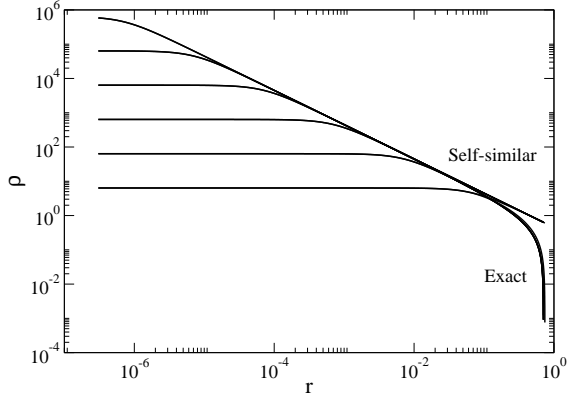


FIG. 4: Evolution of the density profile $\rho(r, t)$ in log-log plot. We have taken $t_{coll} - t = 10^{-6}, 10^{-5}, 10^{-4}, 10^{-3}, 10^{-2}, 10^{-1}$. We have plotted the exact profile (129)-(130) and the self-similar profile (133)-(134) (dashed lines). At $t = t_{coll}$, the exact profiles tend to the density (137) and the self-similar profiles to the density (136). For sufficiently small $t_{coll} - t$, the self-similar profiles and the exact profiles are in good agreement except for $r \sim r_{max}(t)$.

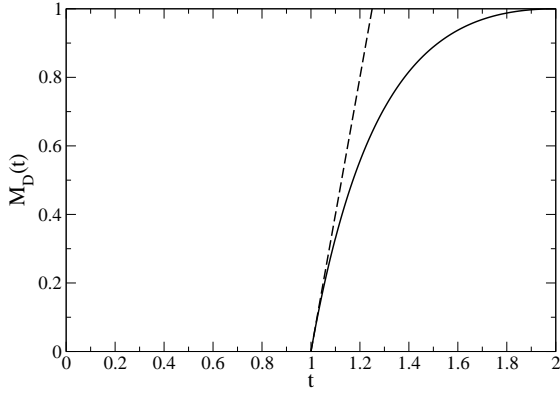


FIG. 5: Evolution of the mass contained in the Dirac peak. The dashed line corresponds to the self-similar solution.

with

$$f(x) = \frac{2}{\pi} \frac{1}{\sqrt{1+2x^2}}. \quad (144)$$

The central residual density corresponding to the self-similar solution (143) is

$$\rho_{ss}(0, t) = \frac{2}{\pi} \frac{1}{t-1}. \quad (145)$$

The singular profile corresponding to the self-similar solution (143) at $t = t_{coll} = 1$ is given by Eq. (136) and the exact density profile at $t = t_{coll} = 1$ is given by Eq. (137). The exact density profile is plotted in Fig. 7 using self-similar variables. This representation illustrates the fact that the solution is self-similar for $t \rightarrow t_{coll} = 1^+$; indeed the curves tends to the invariant profile (144),

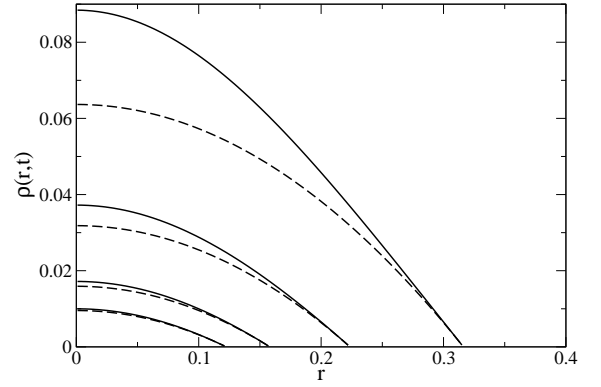


FIG. 6: Evolution of the density for $t \rightarrow t_{end} = 2$. The full line corresponds to the exact profile and the dashed line to the approximation (141). We have represented $t = 1.8, 1.9, 1.95, 1.97$ (top to bottom).

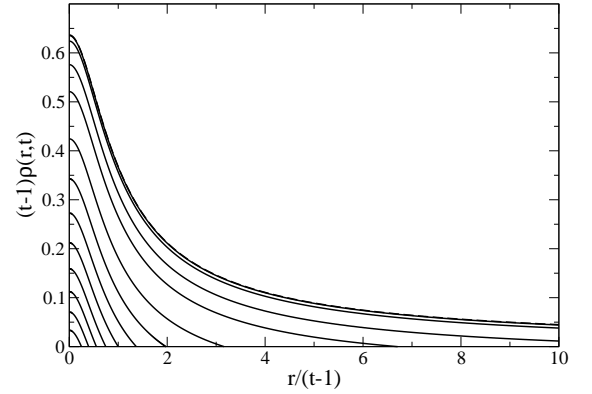


FIG. 7: Evolution of the density profile using self-similar variables. We have taken $t = 1.001, 1.01, 1.05, 1.1, 1.2, 1.3, 1.4, 1.5, 1.6, 1.7, 1.8, 1.9, 2$. The full lines correspond to the exact profile (139)-(140). They tend to the invariant profile (144) represented as a dashed line.

the same as in the pre-collapse regime. Note, however, that the exact central density (142) is different from the self-similar central density (145) [they coincide only for $t \rightarrow t_{coll} = 1^+$], contrary to the pre-collapse regime. This explains why the normalized central density $(t-1)\rho(0, t)$ is not a fixed point in Fig. 7 contrary to Fig. 3. On the other hand, this figure shows the disappearance of the residual density profile at $t = t_{end} = 2$ when all the mass has been absorbed in the Dirac peak at $r = 0$. The exact density profile is also plotted in Fig. 8 in logarithmic variables. This representation illustrates the singularity at $t = t_{coll}$ and the fact that the solution is self-similar for $t \rightarrow t_{coll} = 1^+$. As in the pre-collapse regime, for sufficiently small $t - t_{coll}$, the tail the profile (for $r_0(t) \ll r \ll r_{max}(t)$) is well-approximated by the pure power law (136) but if we want to describe the distribution up to $r_{max}(t) \sim 1/\sqrt{2}$, we must use the truncated

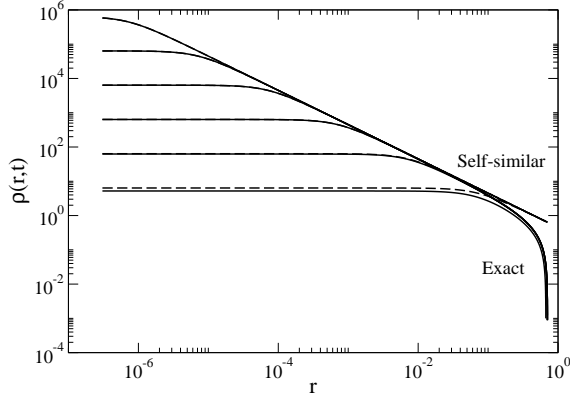


FIG. 8: Evolution of the density profile $\rho(r, t)$ in log-log plot. We have taken $t - t_{coll} = 10^{-6}, 10^{-5}, 10^{-4}, 10^{-3}, 10^{-2}, 10^{-1}$. We have plotted the exact profile (139)-(140) and the self-similar profile (143)-(144) (dashed lines). At $t = t_{coll}$, the exact profile tend to the density (137) and the self-similar profile to the density (136). For sufficiently small $t - t_{coll}$, the self-similar profiles and the exact profiles are in good agreement except for $r \sim r_{max}(t)$. We start to see a difference in the central density for $t - t_{coll} = 0.1$. This difference was imperceptible in the pre-collapse regime for the equivalent time $t_{coll} - t = 0.9$. This is due to the difference in the laws of evolution of the central density (132), (135) [identical] and (142), (145) [different] in the pre and post collapse regimes.

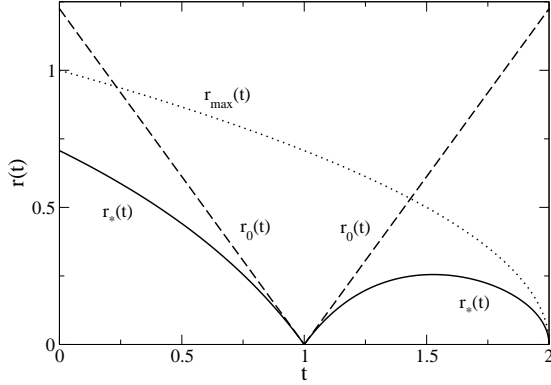


FIG. 9: Evolution of the radii r_{max} (size of the system), r_0 (scaling variable) and r_* (half-central density radius) with time.

power law (137).

We represent in Fig. 9 the evolution of the half central density radius. For $0 \leq t \leq t_{coll} = 1$, it is given by

$$r_*(t) = \frac{1-t}{2-t} \left(2 - \frac{t}{2}\right)^{1/2}, \quad (146)$$

and for $t_{coll} = 1 \leq t \leq t_{end} = 2$, by

$$r_*(t) = \frac{1}{t} \left(\frac{1}{2} + \frac{1}{t}\right)^{1/2} (2-t)^{1/2} (t-1). \quad (147)$$

For $t \rightarrow 0$, we have

$$r_*(t) \simeq \frac{1}{\sqrt{2}} \left(1 - \frac{5t}{8}\right), \quad (148)$$

and for $t \rightarrow t_{end} = 2$,

$$r_*(t) \simeq \frac{1}{2} (2-t)^{1/2}. \quad (149)$$

For $t \rightarrow t_{coll} = 1$, we find that

$$r_*(t) \simeq \left(\frac{3}{2}\right)^{1/2} |t-1|. \quad (150)$$

In the pre-collapse regime, the half central density radius decreases as the profile becomes more and more concentrated. In the post-collapse regime, just after the collapse time t_{coll} , the half central density radius increases as the profile expands, then reaches a maximum and finally decreases to zero as all the particles are absorbed in the Dirac peak. In the self-similar regime, $r_*(t)$ has the same scaling as the core radius $r_0(t)$.

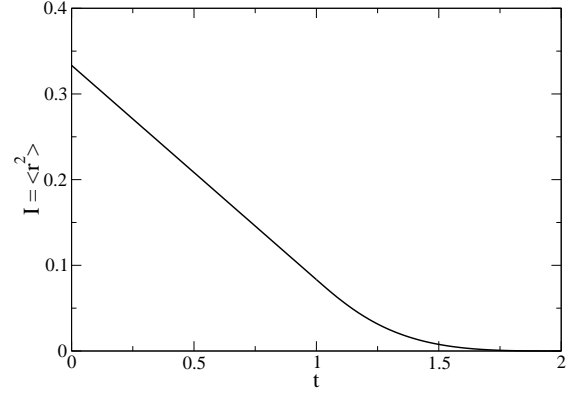


FIG. 10: Evolution of the moment of inertia $I = \langle r^2 \rangle$ with time.

Finally, we represent in Fig. 10 the evolution of the moment of inertia

$$I = \langle r^2 \rangle = \int_0^{r_{max}(t)} \rho(r, t) r^2 2\pi r dr. \quad (151)$$

It can be calculated from Eqs. (129) and (139) after lengthy computations or, more directly, from the virial theorem (B1) of Appendix B. For $0 \leq t \leq t_{coll} = 1$, we find that

$$I(t) = -\frac{t}{4} - \frac{1}{3}, \quad (152)$$

and for $t_{coll} = 1 \leq t \leq t_{end} = 2$, we find that

$$I(t) = \frac{1}{12} \frac{1}{t^3} (2-t)^3 (3t-2). \quad (153)$$

Note that $I(t) = \langle r^2 \rangle(t)$ is a monotonically decreasing function of time.

VII. CONCLUSION

In this paper, we have provided an exact analytical solution describing the gravitational collapse of a gas of self-gravitating Brownian particles in the overdamped limit at $T = 0$. Starting from a parabolic density profile, the system first develops a finite time singularity at $t = t_{coll}$ in the pre-collapse regime, followed by the formation and growth of a Dirac peak in the post-collapse regime. Interestingly, our solution describes all the phases of the dynamics. This extends the purely self-similar solution obtained previously [36–38] that is valid only close to t_{coll} . Unfortunately, our method that exploits the deterministic behavior of the system, is not valid anymore for $T > 0$. In that case, we must resort to other methods [36–39] that are much more complicated. However, the phenomenology of the collapse at $T \neq 0$ (finite time singularity, growth of a Dirac peak, self-similar solutions, pre and post collapse...) remains the same (but, of course, the scaling exponents are different). Therefore, for illustration of the general process of gravitational collapse of self-gravitating Brownian particles, it is useful to have a simple analytical solution such as the one described here.

It is interesting to compare the *isothermal collapse* [36, 45] of self-gravitating Brownian particles in contact with a heat bath to the collapse of isolated stellar systems experiencing a *gravothermal catastrophe* [27, 28]. These two types of systems presents analogies and differences. For both systems, the pre-collapse is self-similar and generates a finite time singularity where the central density is infinite (see [36, 37] for self-gravitating Brownian particles and [46–49] for stellar systems). However, for stellar systems, the post-collapse regime leads to a *binary star* surrounded by a hot halo [46] (statistical equilibrium state in the microcanonical ensemble [25, 28]) instead of a *Dirac peak* containing all the particles [38] (statistical equilibrium state in the canonical ensemble [44, 45]). The binary star can release sufficient energy [46] to stop the collapse and even drive a re-expansion of the system [50]. Then, a series of gravothermal oscillations should follow [51]. More references and discussions about the statistical mechanics of self-gravitating systems in microcanonical and canonical ensembles are given in the reviews [25, 26].

For certain systems, such as those discussed in the Introduction, it is important to take into account both long-range and short-range interactions. As we have seen, due to the attractive long-range interaction, self-gravitating Brownian particles, bacterial populations and colloids driven by attractive capillary interactions can collapse. In that case, the central part of the system becomes very dense. In the absence of short-range interactions, the collapse generically leads to the formation of Dirac peaks. Of course, in practice, Dirac peaks are unphysical and the density profile is regularized by small-scale constraints. These small-scale constraints can be due to finite size effects (the particles always have a finite size and cannot interpenetrate), steric hindrance, short-range

interactions and, ultimately, quantum mechanics (Pauli exclusion principle). These interactions come into play when the system becomes dense enough. Their effect is to provide a nonlinear pressure that can halt the collapse and lead to a well-defined equilibrium state. An example of this regularization is provided by a gas of self-gravitating fermions in which gravitational collapse is balanced by the pressure force arising from the Pauli exclusion principle [21, 26, 52]. Another example is provided by chemotaxis [12] where Dirac peaks are replaced by smooth aggregates. In these examples, the Smoluchowski equation at $T = 0$ studied in this paper must be superseded by more general equations of the form (1) where the pressure $p(\rho)$ prevents complete collapse of the system. A microscopic justification of these equations is given in [2, 3, 13] and some explicit examples of short-range regularization are worked out in [12, 52].

Finally, we would like to point out that the numerous analogies between self-gravitating Brownian particles, chemotaxis, colloids and some nanosystems described in the Introduction lead to the fascinating possibility of reproducing or mimicking a gravitational dynamics and a gravitational collapse in the laboratory. Experimental realizations of these processes will certainly be developed in the future and represent an interesting challenge.

Appendix A: Nonlinear mean field Fokker-Planck equations

The mean field drift-diffusion equation (1) is a subclass of the more general equation

$$\frac{\partial \rho}{\partial t} = \nabla \cdot (Dh(\rho)\nabla \rho + \chi g(\rho)\nabla \Phi), \quad (A1)$$

coupled to Eq. (2) or to a potential $\Phi = \rho * u$ (where $u(\mathbf{r}, \mathbf{r}')$ is a binary potential of interaction and $*$ denotes the convolution product) introduced in [2, 3]. Here, both the diffusion coefficient $Dh(\rho)$ and the mobility $\chi g(\rho)/\rho$ can depend on the density. The fact that the diffusion and the mobility depend on the density in complex systems is not surprising. For example, in a dense fluid, we understand that the motion of a given particle is hampered by interactions with its neighbors so that its mobility is reduced and its diffusivity modified (with respect to a dilute medium). For long-range interactions, these equations generalize the standard Debye-Hückel, Smoluchowski-Poisson and Keller-Segel models. For short-range interactions, we can make the gradient expansion $\Phi \simeq -a\rho - \frac{b}{2}\Delta\rho$ with $a = -S_d \int_0^{+\infty} u(q)q^{d-1} dq$ and $b = -\frac{1}{d}S_d \int_0^{+\infty} u(q)q^{d+1} dq$ [53], and we obtain a generalization of the Cahn-Hilliard equations. Equation (A1) was introduced in [2, 3] as a nonlinear mean field Fokker-Planck equation associated with a generalized thermodynamical formalism. Later, Holm & Putkaradze [32] considered a very related model

$$\frac{\partial \rho}{\partial t} = \nabla \cdot (D\nabla \bar{\rho} + \mu(\bar{\rho})\rho\nabla \Phi), \quad (A2)$$

where $\Phi = \rho * u$ and $\bar{\rho} = \rho * H$, where $u(|\mathbf{r} - \mathbf{r}'|)$ is a binary potential and $H(|\mathbf{r} - \mathbf{r}'|)$ a local filter function. It differs from Eq. (A1) only in the replacement of ρ by $\bar{\rho}$ in the diffusion and mobility terms.

Appendix B: Virial theorem in $d = 2$

In Appendix H of Ref. [54], one of the authors has obtained the proper form of the virial theorem associated with the 2D Smoluchowski-Poisson system which is valid *both* in the pre and post collapse regimes. Its general expression is given by

$$\frac{1}{4}\xi \frac{dI}{dt} = M(t) \left[\frac{k_B T}{m} - \frac{GM_D(t)}{2} - \frac{GM(t)}{4} \right], \quad (\text{B1})$$

where $I = \int \rho r^2 d\mathbf{r} = M \langle r^2 \rangle$ is the moment of inertia, $M_D(t)$ the mass contained in the Dirac peak and $M(t) = M - M_D(t)$ the residual mass contained in the regular density profile. In the absence of Dirac peak, Eq. (B1) reduces to the standard expression [55]:

$$\frac{1}{4}\xi \frac{dI}{dt} = N k_B (T - T_c), \quad (\text{B2})$$

involving the critical temperature

$$k_B T_c = \frac{GMm}{4}. \quad (\text{B3})$$

This equation is *closed* and can be integrated into

$$I(t) = \frac{4Nk_B}{\xi} (T - T_c)t + I_0. \quad (\text{B4})$$

This is valid for any time when $T \geq T_c$ and in the pre-collapse regime when $T < T_c$. In the post-collapse regime when $T < T_c$, we must come back to the general expression (B1). However, this equation is not closed since it involves the mass $M_D(t)$ contained in the Dirac peak. Introducing the mean square displacement $\langle r^2 \rangle = I(t)/M$, Eq. (B4) shows that, for $T \geq T_c$, the motion of a particle is diffusive with an effective diffusion coefficient [55]:

$$D(T) = \frac{k_B T}{\xi m} \left(1 - \frac{T_c}{T} \right), \quad (\text{B5})$$

that is independent on the initial condition.

At $T = 0$, Eq. (B1) reduces to the form

$$\xi \frac{dI}{dt} = -G [M^2 - M_D(t)^2]. \quad (\text{B6})$$

In the pre-collapse regime, $t \leq t_{coll}$, we obtain

$$I(t) = -\frac{GM^2}{\xi} t + I_0. \quad (\text{B7})$$

In the post-collapse regime, $t_{coll} \leq t \leq t_{end}$, we have established in Sec. V that the mass of the Dirac peak increases like (in $d = 2$):

$$M_D(t) = 4M \left(\frac{t_{coll}}{t} \right)^2 \left(\frac{t}{t_{coll}} - 1 \right). \quad (\text{B8})$$

Substituting this expression in Eq. (B6) and integrating Eq. (B6) between t and t_{end} at which $I(t_{end}) = 0$, we find that

$$\frac{I(t)}{MR^2} = \frac{1}{12} \left(\frac{t_{coll}}{t} \right)^3 \left(2 - \frac{t}{t_{coll}} \right)^3 \left(\frac{3t}{t_{coll}} - 2 \right). \quad (\text{B9})$$

We have checked, after lengthy calculations, that Eqs. (B7) and (B9) can also be obtained directly from the exact analytical density profiles (75) and (120). The evolution of the moment of inertia (proportional to the dispersion of the particles) is plotted in Fig. 10.

There is no closed expression of the virial theorem when $d \neq 2$. Therefore, the moment of inertia must be calculated directly from the exact analytical expressions of the density profile given in the main part of the paper. We shall give only particular values of the moment of inertia in d dimensions

$$I(t) = \int_0^{r_{max}(t)} \rho(r, t) r^2 S_d r^{d-1} dr. \quad (\text{B10})$$

For $t \rightarrow 0$, using Eqs. (49) and (51), we find that

$$I(t) \simeq I_0 - \frac{12}{(d+4)(d+6)} MR^2 \frac{t}{t_{coll}}. \quad (\text{B11})$$

For $t = t_{coll}$, using Eqs. (54) and (55), we get

$$I(t_{coll}) = \frac{d^3}{d+2} \left(\frac{d}{d+2} \right)^{2/d} \frac{1}{d^2 + 2d + 4} MR^2. \quad (\text{B12})$$

For $t \rightarrow t_{end}$, using Eqs. (100) and (102), we obtain

$$I(t) \sim \frac{d(d+2)}{2(d^2 + 3d + 2)} MR^2 \left(\frac{t_{end} - t}{t_{end}} \right)^{2(d+1)/d}. \quad (\text{B13})$$

Using Eqs. (102) and (103), we check that this last expression can be written

$$I(t) \sim \frac{d^2}{d^2 + 3d + 2} M(t) r_{max}(t)^2. \quad (\text{B14})$$

For $d = 2$, the expressions (B11), (B12) and (B13) are consistent with the general results (B7) and (B9) valid for all times. For the uniform sphere in d dimension, using Eqs. (26)-(28), we obtain

$$I(t) = \frac{d}{d+2} MR^2 \left(1 - \frac{dGM}{\xi R^d} t \right)^{2/d} = \frac{d}{d+2} MR(t)^2. \quad (\text{B15})$$

In $d = 2$, this expression reduces to Eq. (B7) as it should.

Appendix C: Derivation of the generalized mean field Smoluchowski equation

In this Appendix, following [13], we provide a new derivation of the generalized mean field Smoluchowski

equation (1). In previous works [2, 3, 10], this equation was derived from a notion of generalized thermodynamics. In that case, the nonlinear pressure was due to a bias in the transition probabilities leading to non-Boltzmannian distributions [9]. Here, we show that the same equation can be derived from the Dynamic Density Functional Theory (DDFT) used in the theory of simple liquids [56]. In that case, the nonlinear pressure is due to the correlations induced by the short-range interactions. Although physically distinct, these processes lead to the same type of macroscopic equations. A more detailed discussion, as well as the derivation of more general kinetic equations, is given in [13].

We consider the overdamped dynamics of N Brownian particles in interaction governed by the coupled stochastic equations [7]:

$$\frac{d\mathbf{r}_i}{dt} = -\mu \nabla_i U(\mathbf{r}_1, \dots, \mathbf{r}_N) + \sqrt{2D} \mathbf{R}_i(t), \quad (\text{C1})$$

where $U(\mathbf{r}_1, \dots, \mathbf{r}_N) = m^2 \sum_{i < j} u(|\mathbf{r}_i - \mathbf{r}_j|)$ is the potential of interaction and $\mathbf{R}_i(t)$ is a Gaussian white noise such that $\langle \mathbf{R}_i(t) \rangle = \mathbf{0}$ and $\langle R_i^\alpha(t) R_j^\beta(t') \rangle = \delta_{ij} \delta_{\alpha\beta} \delta(t-t')$. Here, $i = 1, \dots, N$ label the particles and $\alpha = 1, \dots, d$ the coordinates of space. The diffusion coefficient D is related to the mobility $\mu = 1/(\xi m)$ and the temperature T by the Einstein relation $D = \mu k_B T$ [5]. The time evolution of the N -body distribution $P_N(\mathbf{r}_1, \dots, \mathbf{r}_N, t)$ is governed by the N -body Fokker-Planck equation

$$\xi \frac{\partial P_N}{\partial t} = \sum_{i=1}^N \frac{\partial}{\partial \mathbf{r}_i} \cdot \left[\frac{k_B T}{m} \frac{\partial P_N}{\partial \mathbf{r}_i} + \frac{1}{m} P_N \frac{\partial}{\partial \mathbf{r}_i} U(\mathbf{r}_1, \dots, \mathbf{r}_N) \right]. \quad (\text{C2})$$

This particular Fokker-Planck equation is called the N -body Smoluchowski equation. Its steady state is the Gibbs canonical distribution $P_N = \frac{1}{Z} e^{-\beta U}$.

It is easy to derive from Eq. (C2) the equivalent of the BBGKY hierarchy for the reduced distribution functions [7]. Introducing the local density $\rho(\mathbf{r}, t) = N m P_1(\mathbf{r}, t)$ and the two-body distribution function $\rho_2(\mathbf{r}, \mathbf{r}', t) = N(N-1) m^2 P_2(\mathbf{r}, \mathbf{r}', t)$, the first equation of the BBGKY-like hierarchy is the exact Smoluchowski equation

$$\xi \frac{\partial \rho}{\partial t} = \nabla \cdot \left[\frac{k_B T}{m} \nabla \rho + \int \rho_2(\mathbf{r}, \mathbf{r}', t) \nabla u(|\mathbf{r} - \mathbf{r}'|) d\mathbf{r}' \right], \quad (\text{C3})$$

where we have used the fact that the particles are identical. This equation is not closed since it involves the two-body correlation function $\rho_2(\mathbf{r}, \mathbf{r}', t)$. We must therefore introduce some approximations to evaluate this term. We shall assume that the potential of interaction $u = u_{LR} + u_{SR}$ is the sum of a long-range potential u_{LR} and a short-range potential u_{SR} . For systems with long-range interactions, it is known that the mean field approximation is exact in a proper thermodynamic limit $N \rightarrow +\infty$ [6, 57]. Therefore, concerning the long-range potential u_{LR} , we shall make the approximation

$\rho_2(\mathbf{r}, \mathbf{r}', t) = \rho(\mathbf{r}, t) \rho(\mathbf{r}', t)$ leading to

$$\int \rho_2(\mathbf{r}, \mathbf{r}', t) \nabla u_{LR}(|\mathbf{r} - \mathbf{r}'|) d\mathbf{r}' = \rho(\mathbf{r}, t) \nabla \Phi(\mathbf{r}, t), \quad (\text{C4})$$

with

$$\Phi(\mathbf{r}, t) = \int \rho(\mathbf{r}', t) u_{LR}(|\mathbf{r} - \mathbf{r}'|) d\mathbf{r}'. \quad (\text{C5})$$

To evaluate the integral corresponding to the short-range interactions, we shall use an approximation that has become standard in the dynamic density functional theory (DDFT) of fluids [56] and take

$$\int \rho_2(\mathbf{r}, \mathbf{r}', t) \nabla u_{SR}(|\mathbf{r} - \mathbf{r}'|) d\mathbf{r}' \simeq \rho(\mathbf{r}, t) \nabla \frac{\delta F_{ex}}{\delta \rho}[\rho(\mathbf{r}, t)], \quad (\text{C6})$$

where $F_{ex}[\rho]$ is the excess free energy [66] calculated at equilibrium. This relation is exact at equilibrium [58] and the approximation consists in extending it out-of-equilibrium with the actual density $\rho(\mathbf{r}, t)$ calculated at each time. This closure is equivalent to assuming that the two-body dynamic correlations are the same as those in an equilibrium fluid with the same one body density profile. Although it is not possible to ascertain the validity of this approximation in the general case, it has been observed for the systems considered that this approximation gives remarkable agreement with direct Brownian N -body simulations. With the approximations (C4) and (C6), Eq. (C3) becomes

$$\xi \frac{\partial \rho}{\partial t} = \nabla \cdot \left[\frac{k_B T}{m} \nabla \rho + \rho \nabla \frac{\delta F_{ex}}{\delta \rho} + \rho \nabla \Phi \right], \quad (\text{C7})$$

which is closed. The total free energy is

$$F[\rho] = \frac{1}{2} \int \rho \Phi d\mathbf{r} + k_B T \int \frac{\rho}{m} \ln \frac{\rho}{m} d\mathbf{r} + F_{ex}[\rho]. \quad (\text{C8})$$

The steady state of Eq. (C7) minimizes (C8) at fixed mass and is given by $\delta F - \mu \delta M = 0$ where μ is a Lagrange multiplier. This yields $\delta F / \delta \rho = \mu$ i.e.

$$\rho(\mathbf{r}) = A e^{-\beta m (\Phi + \frac{\delta F_{ex}}{\delta \rho})}. \quad (\text{C9})$$

In a fluid, the local pressure is of the form $p = p(\rho, T)$. Since the temperature T is fixed in the case of Brownian particles (canonical description), the pressure is barotropic and we shall simply write $p = p(\rho)$. In principle, the excess free energy $F_{ex}[\rho]$ can depend on the gradients of the density. This is particularly important for a fluid close to an interface [58]. Here, we shall assume that the density varies on a distance that is large with respect to the range of intermolecular forces. This is the case if the density distribution is mainly due to long-range interactions, as we shall assume in the following. With this assumption, the free energy is of the form [13]:

$$F[\rho] = \frac{1}{2} \int \rho \Phi d\mathbf{r} + \int \rho \int^\rho \frac{p(\rho_1)}{\rho_1^2} d\rho_1 d\mathbf{r}. \quad (\text{C10})$$

The excess free energy is therefore

$$F_{ex}[\rho] = \int \rho \int \frac{p(\rho_1)}{\rho_1^2} d\rho_1 d\mathbf{r} - k_B T \int \frac{\rho}{m} \ln \frac{\rho}{m} d\mathbf{r}. \quad (\text{C11})$$

We note the relation

$$\nabla p(\rho) = \frac{k_B T}{m} \nabla \rho + \rho \nabla \frac{\delta F_{ex}}{\delta \rho} = \nabla p_{id} + \nabla p_{ex}, \quad (\text{C12})$$

where $p_{id}(\mathbf{r}) = \rho(\mathbf{r})k_B T/m$ is the ideal gas law and p_{ex} the excess pressure due to short-range interactions [59]. This relation can be used to determine the equation of state $p(\rho)$ corresponding to the excess free energy $F_{ex}[\rho]$ and *vice versa*. For an ideal fluid ($F_{ex} = 0$), we recover the perfect gas law $p(\mathbf{r}) = \rho(\mathbf{r})k_B T/m$. For a free energy of the form (C10), using identity (C12), Eq. (C7) can be rewritten

$$\xi \frac{\partial \rho}{\partial t} = \nabla \cdot (\nabla p + \rho \nabla \Phi). \quad (\text{C13})$$

The equilibrium state is given by the condition of hydrostatic equilibrium

$$\nabla p + \rho \nabla \Phi = \mathbf{0}. \quad (\text{C14})$$

Equation (C13) is a generalized mean field Smoluchowski equation including a generically nonlinear barotropic pressure $p(\rho)$ due to short-range interactions and a mean field potential $\Phi = u_{LR} * \rho$ due to long-range interactions. As we have indicated in the Introduction, this equation arises in several physical problems such as self-gravitating Brownian particles [1], chemotaxis [29], colloids with capillary interactions [30], etc. Combining results issued from the physics of systems with long-range interactions [6] and from the dynamic density functional theory of fluids [56], this equation has been justified from a microscopic model [13].

The generalized mean field Smoluchowski equation (C7) can be written in terms of the free energy functional (C8) as

$$\frac{\partial \rho}{\partial t} = \nabla \cdot \left(\frac{1}{\xi} \rho \nabla \frac{\delta F}{\delta \rho} \right). \quad (\text{C15})$$

This equation monotonically decreases the free energy functional (C8) which plays therefore the role of a Lyapunov functional. Indeed, a straightforward calculation leads to the H -theorem appropriate to the canonical ensemble

$$\begin{aligned} \dot{F} &= \int \frac{\delta F}{\delta \rho} \frac{\partial \rho}{\partial t} d\mathbf{r} = \int \frac{\delta F}{\delta \rho} \nabla \cdot \left(\frac{1}{\xi} \rho \nabla \frac{\delta F}{\delta \rho} \right) d\mathbf{r} \\ &= - \int \frac{1}{\xi} \rho \left(\nabla \frac{\delta F}{\delta \rho} \right)^2 d\mathbf{r} \leq 0. \end{aligned} \quad (\text{C16})$$

For a steady state, $\dot{F} = 0$, the last term in parenthesis must vanish so that $\delta F/\delta \rho$ is uniform. This leads to Eq. (C9). Therefore, a density $\rho(\mathbf{r})$ is a steady state of the

generalized mean field Smoluchowski equation (C15) iff it is a critical point of F at fixed mass. Furthermore, it can be shown that a steady state is linearly dynamically stable with respect to the generalized Smoluchowski equation (C15) iff it is a (local) minimum of F at fixed mass [3, 4]. This is consistent with the condition of thermodynamical equilibrium. If F is bounded from below [67], we know from Lyapunov's direct method that the system will converge towards a (local) minimum of F at fixed mass M for $t \rightarrow +\infty$. If several (local) minima exist (metastable states), the choice of the selected equilibrium will depend on a complicated notion of basin of attraction.

Remark: note that Eq. (C15) can be justified in a phenomenological manner from the linear thermodynamics of Onsager if we interpret it as a continuity equation $\partial_t \rho + \nabla \cdot \mathbf{J} = 0$ with a current $\mathbf{J} = -(1/\xi) \nabla \delta F/\delta \rho$ proportional to the gradient of a potential $\mu(\mathbf{r}) = \delta F/\delta \rho$ that is uniform at equilibrium (see Eq. (C9)). This is precisely the way in which this equation was introduced in the physics of liquids [58] and, more generally, in [3, 4].

Appendix D: The formation of a peripheric Dirac peak

In Sec. II we have mentioned that the evolution of the system is qualitatively different whether $M(a, 0)/a^d$ is an increasing or a decreasing function of a . In the main part of the paper, we have considered the physical situation where $M(a, 0)/a^d$ decreases. We have shown that such initial conditions lead to the growth of a Dirac peak at the origin. In this Appendix, we illustrate on a specific example the situation where $M(a, 0)/a^d$ increases. We show that such initial conditions lead to the formation of a peripheric Dirac peak (a d -dimensional annulus) that progressively converges towards the center of the domain by absorbing the interior particles. To simplify the formulae, we choose a system of units such that $M = \xi = G = 1$. We also assume that the initial size of the system is $R = 1$.

An analytical solution can be obtained by considering an initial condition of the form

$$M(a, 0) = a^{2d}, \quad (\text{D1})$$

for $a \leq 1$ and $M(a, 0) = 1$ for $a \geq 1$. The corresponding density profile, given by Eq. (18), is

$$\rho(a, 0) = \frac{2d}{S_d} a^d, \quad (\text{D2})$$

for $a \leq 1$ and $\rho(a, 0) = 0$ for $a \geq 1$. The density increases with the radius for $a \leq 1$ and vanishes discontinuously at $a = 1$. According to Eq. (21), the position at time t of the particle initially located at a is

$$r^d = a^d - da^{2d}t. \quad (\text{D3})$$

According to Eqs. (19) and (D1), the mass profile at time t is

$$M(r, t) = a^{2d}, \quad (\text{D4})$$

where a is related to r and t through Eq. (D3). The size of the system at time t , i.e. the position of the last particle initially located at $a = 1$, is

$$r_{max}(t) = (1 - dt)^{1/d}. \quad (\text{D5})$$

From Eq. (D5), all the particles have collapsed at $r = 0$ at the final time

$$t_{end} = \frac{1}{d}. \quad (\text{D6})$$

Solving for a in Eq. (D3), which is a second degree equation in a^d , and substituting the resulting expression in Eq. (D4), we obtain

$$M(r, t) = \frac{1}{(2dt)^2} \left(1 - \sqrt{1 - 4dtr^d} \right)^2. \quad (\text{D7})$$

According to Eq. (18), the corresponding density profile is

$$\rho(r, t) = \frac{1}{S_d t} \left(\frac{1}{\sqrt{1 - 4dtr^d}} - 1 \right). \quad (\text{D8})$$

It is represented in Fig. 11 at different times. Since $r \leq r_{max}(t)$, we can check that the term under the square root is always positive. It vanishes for $r = r_{max}$ at the collapse time

$$t_{coll} = \frac{1}{2d}. \quad (\text{D9})$$

At that time, the density becomes infinite at $r = r_{max}(t_{coll}) = (1/2)^{1/d}$. On the other hand, we note that the central density $\rho(0, t) = 0$ at any time. The density profile is self-similar since

$$\rho(r, t) = \frac{1}{t} f(rt^{1/d}), \quad (\text{D10})$$

with the invariant profile

$$f(x) = \frac{1}{S_d} \left(\frac{1}{\sqrt{1 - 4dx^d}} - 1 \right). \quad (\text{D11})$$

This function increases and diverges when $x \rightarrow (1/4d)^{1/d}$. We must distinguish two cases:

(i) For $t < t_{coll}$, a simple calculation shows that

$$\rho(r_{max}(t), t) = \frac{2d}{S_d} \frac{1}{1 - 2dt}, \quad (\text{D12})$$

$$M(r_{max}(t), t) = 1. \quad (\text{D13})$$

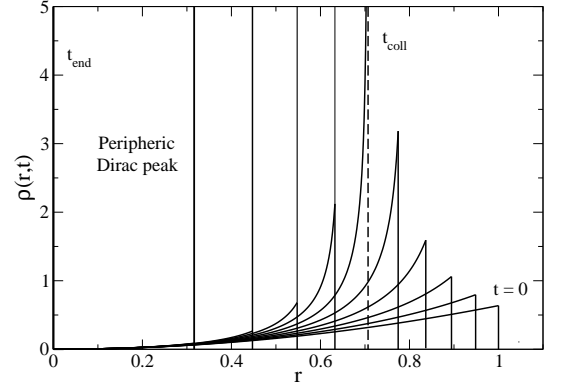


FIG. 11: Evolution of the density profile $\rho(r, t)$ in $d = 2$. The time t goes from 0 to $t_{end} = 0.5$ and is represented every 0.05 time steps. The vertical line corresponds to the peripheral Dirac peak, appearing at $t = t_{coll} = 1/4$ and containing all the mass at $t = t_{end} = 1/2$.

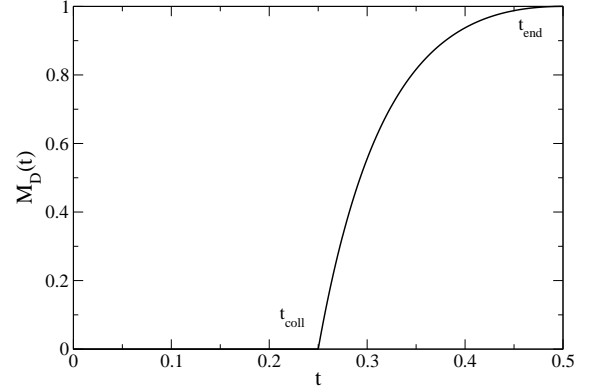


FIG. 12: Evolution of the mass contained in the peripheral Dirac peak in $d = 2$.

In that case, the profile (D7)-(D8) contains all the mass and there is no Dirac peak. The density at the periphery $\rho(r_{max}(t), t)$ increases monotonically with time and diverges when $t = t_{coll}$. The density profile at $t = t_{coll}$ is

$$\rho(r, t_{coll}) = \frac{2d}{S_d} \left(\frac{1}{\sqrt{1 - 2r^d}} - 1 \right), \quad (\text{D14})$$

for $r < r_{max}(t_{coll}) = (1/2)^{1/d}$ and $\rho(r, t) = 0$ otherwise.

(ii) For $t > t_{coll}$, a simple calculation shows that

$$\rho(r_{max}(t), t) = \frac{2}{S_d t} \frac{1 - dt}{2dt - 1}, \quad (\text{D15})$$

$$M(r_{max}(t), t) = \frac{1}{(dt)^2} (1 - dt)^2. \quad (\text{D16})$$

In that case, the profile (D7)-(D8) does *not* contain all the mass. A Dirac peak forms at $r = r_{max}(t)$ and captures the peripheral mass as the system shrinks. The mass

contained in the Dirac peak is $M_D(t) = 1 - M(r_{max}(t), t)$ yielding

$$M_D(t) = \frac{2dt - 1}{(dt)^2}. \quad (D17)$$

It obviously satisfies $M_D(t_{coll}) = 0$ and $M_D(t_{end}) = 1$ (see Fig. 12). The density at the periphery is infinite at $t = t_{coll}$ and monotonically decreases for $t > t_{coll}$ as the Dirac peak grows by absorbing the neighboring particles. The total (normalized) density profile can be written

$$\rho_{tot}(\mathbf{r}, t) = \rho(\mathbf{r}, t) + M_D(t) \frac{\delta(r - r_{max}(t))}{S_d r^{d-1}}, \quad (D18)$$

where the first term $\rho(\mathbf{r}, t)$ is the regular density profile (D8) and the second term corresponds to the Dirac peak. For $t \rightarrow t_{coll}$ and $r \rightarrow r_{max}(t)^-$, the regular density profile (D8) has the self-similar form

$$\rho(r, t) = \frac{1}{|t - t_{coll}|} \frac{1}{S_d \sqrt{1 + \frac{2^{1/d-2} r_{max}(t) - r}{d(t - t_{coll})^2}}}. \quad (D19)$$

We can understand the onset of the Dirac peak formation in a more qualitative manner. According to Eq. (D3), the positions of the particles initially located at a_1 and $a_2 > a_1$ coincide at the time

$$t = \frac{1}{d} \frac{1}{a_1^d + a_2^d}, \quad (D20)$$

and take the value

$$r_1 = r_2 = \frac{a_1 a_2}{(a_1^d + a_2^d)^{1/d}}. \quad (D21)$$

The shortest time at which this coincidence occurs corresponds to $a_1 \sim a_2 \sim 1$ yielding $t = t_{coll} = 1/(2d)$ and $r_1 = r_2 = (1/2)^{1/d}$. At that time, the density becomes infinite since there is a finite mass in the interval $r_2 - r_1 \rightarrow 0$. Then, a peripheric Dirac peak with mass $M_D(t)$ forms at $r_{max}(t)$ and grows by capturing the neighboring particles as the system collapses. At $t = t_{end}$, the Dirac annulus has reached the origin and all the particles are contained in a central Dirac peak at $r = 0$.

Remark: According to Eq. (D3), we would naively conclude that the particle initially at a reaches the origin $r = 0$ at time $t_*(a) = 1/(da^d)$. This time decreases with a so that the particles that are initially close to the origin seem to take more time to collapse at $r = 0$ than far away particles. In particular, for $a < 1$, we find that $t_*(a) > t_{end}$ which leads to an apparent paradox. In fact, the above estimate is not correct. Indeed, a particle initially located at a is captured by the peripheric Dirac peak at a time $t_c(a)$ such that $r(t_c(a)) = r_{max}(t_c(a))$. This leads to $t_c(a) = (1 - a^d)/[d(1 - a^{2d})]$. For $a \rightarrow 1$, we find that $t_c(a) \rightarrow t_{coll} = 1/(2d)$ which corresponds to the onset of the peripheric Dirac peak. We also note that $t_c(a) < t_*(a)$ for $a \leq 1$, so that the particles are captured

by the peripheric Dirac peak before they can reach the origin according to their pure motion (D3). Therefore, they are carried towards the origin by the Dirac peak whose equation of motion is given by Eq. (D5). This solves the apparent paradox.

Appendix E: Repulsive interaction

In the main part of the paper, we have considered the situation where the interaction between particles is attractive like gravity ($G > 0$). In this Appendix, we briefly consider the case of a repulsive interaction like in a Coulombian plasma ($G < 0$). In chemotaxis, when the chemical substance secreted by the biological entities acts as a *pheromone*, the interaction is attractive (chemoattraction) but when it acts as a *poison*, the interaction is repulsive (chemorepulsion). The case of a repulsive interaction can therefore have interesting physical applications.

In the deterministic case ($T = 0$), the general exact solution of the problem is given by Eqs. (19) and (21) by simply making the substitution $G \rightarrow -G$. Accordingly, the dynamical evolution of a uniform sphere is given by Eqs. (23)-(29) with G replaced by $-G$. The sphere remains uniform during the evolution but it now expands instead of collapsing. The mass profile, the radius and the density evolve like

$$M(r, t) = \frac{M}{R^d} \frac{r^d}{1 + \frac{dGM}{\xi R^d} t}, \quad (E1)$$

$$R(t) = R \left(1 + \frac{dGM}{\xi R^d} t \right)^{1/d}, \quad (E2)$$

$$\rho(t) = \frac{\rho(0)}{1 + \frac{dGM}{\xi R^d} t}. \quad (E3)$$

For $t \rightarrow +\infty$, we obtain the scalings $M(r, t) \sim \xi r^d / (dGt)$, $R(t) \sim (dGMt/\xi)^{1/d}$ and $\rho(t) \sim \xi / (S_d Gt)$.

For the initial parabolic profile (30)-(33), the exact time dependent solution can be written

$$M(r, t) = Aa^d(1 - Ba^2), \quad (E4)$$

$$x^d = \frac{d}{\xi} GAa^d(1 - Ba^2) + \frac{a^d}{t}, \quad (E5)$$

$$x = \frac{r}{t^{1/d}}. \quad (E6)$$

The corresponding density profile is

$$\rho(r, t) = \frac{\xi}{S_d Gt} \frac{1 - \frac{a^2}{R^2}}{1 - \frac{a^2}{R^2} + \frac{\xi}{dGAt}}. \quad (E7)$$

The size of the system, i.e. the position of the last particle initially located at $a = R$ at time $t = 0$, is

$$r_{max}(t) = R \left(1 + \frac{dGM}{\xi R^d} t \right)^{1/d}. \quad (\text{E8})$$

We note that this expression coincides with Eq. (E2) for all times. The central density ($r = a = x = 0$) decreases like

$$\rho(0, t) = \frac{\xi}{S_d G t} \frac{1}{1 + \frac{\xi}{d G A t}}. \quad (\text{E9})$$

For $t \rightarrow +\infty$, the system behaves like a homogeneous sphere since Eqs. (E4)-(E9) become equivalent to Eqs. (E1)-(E3) in this limit. Considering the general equations of the problem, we note that this property is valid for an arbitrary initial profile. For $t \rightarrow 0$, we find that

$$\begin{aligned} \rho(r, t) &\simeq \rho(r, 0) - \frac{d^2(d+2)^2}{4S_d} \frac{GM^2}{\xi R^{2d}} \\ &\times \left[1 - \frac{2(d+1)}{d} \frac{r^2}{R^2} + \frac{d+4}{d+2} \frac{r^4}{R^4} \right] t. \end{aligned} \quad (\text{E10})$$

The corresponding mass profile is

$$\begin{aligned} M(r, t) &\simeq M(r, 0) - \frac{d(d+2)^2}{4} \frac{GM^2}{\xi R^{2d}} r^d \\ &\times \left[1 - \frac{2(d+1)}{d+2} \frac{r^2}{R^2} + \frac{d}{d+2} \frac{r^4}{R^4} \right] t. \end{aligned} \quad (\text{E11})$$

These expressions are valid for $r \leq r_{max}(t)$ with

$$r_{max}(t) \simeq R \left(1 + \frac{GMt}{\xi R^d} \right). \quad (\text{E12})$$

For $t \rightarrow 0$, the central density evolves like

$$\rho(0, t) \simeq \frac{dA}{S_d} \left(1 - \frac{dGAt}{\xi} \right). \quad (\text{E13})$$

In $d = 2$, Eq. (E5) can be solved explicitly to obtain $a(x, t)$. We get

$$a^2 = \frac{1}{2B} \left[1 + \frac{\xi}{2GAt} - \sqrt{\left(1 + \frac{\xi}{2GAt} \right)^2 - \frac{2\xi B x^2}{GA}} \right]. \quad (\text{E14})$$

Substituting this expression in Eqs. (E4) and (E7), we obtain an explicit solution for $M(r, t)$ and $\rho(r, t)$. To simplify the notations, we introduce dimensionless variables such that $M = R = 1$, $A = 2$, $B = 1/2$, $\xi/G = 4$ and $S_2 = 2\pi$ like in Sec. VI. Equations (E7) and (E14) can be combined to give

$$\rho(r, t) = \frac{2}{\pi t} \left(1 - \frac{1}{\sqrt{(1+t)^2 - 2r^2 t}} \right), \quad (\text{E15})$$

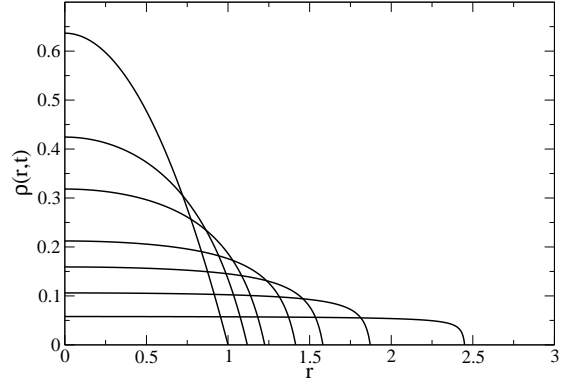


FIG. 13: Evolution of the density profile $\rho(r, t)$ in $d = 2$ for $t = 0, 0.5, 1, 2, 3, 5, 10$. The initial density profile is parabolic but it asymptotically tends towards a step function (uniform disk).

for $r \leq r_{max}(t)$ with

$$r_{max}(t) = \left(1 + \frac{t}{2} \right)^{1/2}. \quad (\text{E16})$$

For $r \geq r_{max}(t)$, we have $\rho(r, t) = 0$ as usual. The density profile is plotted in Fig. 13 for different times. For $t = 0$, the profile is parabolic and for $t \rightarrow +\infty$, it tends to a Heaviside function (uniform disk). The central density decreases like

$$\rho(0, t) = \frac{2}{\pi} \frac{1}{1+t}. \quad (\text{E17})$$

In the repulsive case, making the substitution $G \rightarrow -G$ in Eqs. (B2)-(B3), the virial theorem in $d = 2$ dimensions reads

$$\frac{1}{4} \xi \frac{dI}{dt} = N \left(k_B T + \frac{GMm}{4} \right). \quad (\text{E18})$$

It can be integrated into

$$I(t) = \frac{4N}{\xi} \left(k_B T + \frac{GMm}{4} \right) t + I(0). \quad (\text{E19})$$

For $T = 0$, we obtain

$$I(t) = \frac{GM^2}{\xi} t + I(0). \quad (\text{E20})$$

Introducing the mean square displacement $\langle r^2 \rangle = I(t)/M$, Eq. (E19) shows that the motion of a particle is diffusive with an effective diffusion coefficient

$$D(T) = \frac{k_B T}{\xi m} + \frac{GM}{4\xi}, \quad (\text{E21})$$

that is independent on the initial condition. For $T = 0$, we obtain $D_0 = GM/(4\xi)$. For the uniform sphere in d

dimension, using Eqs. (E1)-(E3), we get

$$I(t) = \frac{d}{d+2} MR^2 \left(1 + \frac{dGM}{\xi R^d} t \right)^{2/d} = \frac{d}{d+2} MR(t)^2. \quad (\text{E22})$$

In $d = 2$, this expression reduces to Eq. (E20) as it should. For a parabolic initial condition, introducing the

dimensionless variables defined previously and using Eq. (E15), we find after some calculations that

$$I(t) = \langle r^2 \rangle = \frac{t}{4} + \frac{1}{3}. \quad (\text{E23})$$

This expression coincides with Eq. (E20), as it should.

-
- [1] C. Sire and P.H. Chavanis, *Collapse and evaporation of a canonical self-gravitating gas* in Proceedings of the 12th Marcel Grossmann Meeting (World Scientific, Singapore, 2010) [arXiv:1003.1118]
 - [2] P.H. Chavanis, Phys. Rev. E **68**, 036108 (2003)
 - [3] P.H. Chavanis, Eur. Phys. J. B **62**, 179 (2008)
 - [4] T.D. Frank, *Nonlinear Fokker-Planck Equations: Fundamentals and Applications* (Springer-Verlag, 2005)
 - [5] H. Risken, *The Fokker-Planck equation* (Springer, 1989)
 - [6] A. Campa, T. Dauxois, S. Ruffo, Physics Reports **480**, 57 (2009)
 - [7] P.H. Chavanis, Physica A **361**, 81 (2006)
 - [8] L. Borland, Phys. Rev. E **57**, 6634 (1998)
 - [9] G. Kaniadakis, Physica A **296**, 405 (2001)
 - [10] P.H. Chavanis, P. Laurençot, M. Lemou, Physica A **341**, 145 (2004)
 - [11] C. Tsallis, J. Stat. Phys. **52**, 479 (1988)
 - [12] P.H. Chavanis, Eur. Phys. J. B **54**, 525 (2006)
 - [13] P.H. Chavanis, Physica A **390**, 1546 (2011)
 - [14] H. Spohn, J. Physique **3**, 69 (1993)
 - [15] A.R. Plastino, A. Plastino, Physica A **222**, 347 (1995)
 - [16] P. Debye, E. Hückel, Phys. Z. **24**, 305 (1923)
 - [17] P. Biler, J. Dolbeault, Ann. Henri Poincaré **1**, 461 (2000)
 - [18] V. Barcion, D.P. Chen, R.S. Eisenberg, SIAM J. Appl. Math. **52**, 1405 (1992)
 - [19] A. Syganow, E. von Kitzing, J. Phys. Chem. **99**, 12030 (1995)
 - [20] A.M. Anile, V. Romano, G. Russo, SIAM J. Appl. Math. **61**, 74 (2000)
 - [21] S. Chandrasekhar, *An Introduction to the Theory of Stellar Structure* (Dover, 1942)
 - [22] J. Binney, S. Tremaine, *Galactic Dynamics* (Princeton Series in Astrophysics, 1987)
 - [23] L. Spitzer, *Dynamical Evolution of Globular Clusters* (Princeton Series in Astrophysics, 1987)
 - [24] P.H. Chavanis, A&A **356**, 1089 (2000)
 - [25] T. Padmanabhan, Physics Reports **188**, 285 (1990)
 - [26] P.H. Chavanis, Int J. Mod. Phys. B **20**, 3113 (2006)
 - [27] V.A. Antonov, Vest. Leningr. Gos. Univ. **7**, 135 (1962)
 - [28] D. Lynden-Bell, R. Wood, Mon. not. R. astron. Soc. **138**, 495 (1968)
 - [29] E.F. Keller, L.A. Segel, J. Theor. Biol. **30**, 225 (1971)
 - [30] A. Dominguez, M. Oettel, S. Dietrich, Phys. Rev. E **82**, 011402 (2010)
 - [31] G. Giacomin, J. Lebowitz, Phys. Rev. Lett. **76**, 1094 (1996)
 - [32] D. Holm, V. Putkaradze, Phys. Rev. Lett. **95**, 226106 (2005)
 - [33] R. Robert, J. Sommeria, Phys. Rev. Lett. **69**, 2776 (1992)
 - [34] P.H. Chavanis, J. Sommeria, R. Robert, Astrophys. J. **471**, 385 (1996)
 - [35] P.H. Chavanis, *Statistical mechanics of two-dimensional vortices and stellar systems*, in: Dynamics and thermodynamics of systems with long range interactions, edited by Dauxois, T., Ruffo, S., Arimondo, E. and Wilkens, M. Lect. Not. in Phys. **602** (Springer, 2002)
 - [36] P.H. Chavanis, C. Rosier, C. Sire, Phys. Rev. E **66**, 036105 (2002)
 - [37] C. Sire, P.H. Chavanis, Phys. Rev. E **66**, 046133 (2002)
 - [38] C. Sire, P.H. Chavanis, Phys. Rev. E **69**, 066109 (2004)
 - [39] P. Lushnikov, Physics Letters A **374**, 1678 (2010)
 - [40] C. Hunter, Astrophys. J. **136**, 594 (1962)
 - [41] L. Mestel, Q. Jl. R. astr. Soc. **144**, 425 (1969)
 - [42] M.V. Penston, Mon. not. R. astron. Soc. **144**, 425 (1969)
 - [43] D. Lynden-Bell, Mon. not. R. astron. Soc. **136**, 101 (1967)
 - [44] M. Kiessling, J. Stat. Phys. **55**, 203 (1989)
 - [45] P.H. Chavanis, A&A **381**, 340 (2002)
 - [46] M. Hénon, Ann. Astrophys. **24**, 369 (1961)
 - [47] D. Lynden-Bell, P.P. Eggleton, Mon. not. R. astron. Soc. **191**, 483 (1980)
 - [48] H. Cohn, Astrophys. J. **242**, 765 (1980)
 - [49] C. Lancellotti, M. Kiessling, Astrophys. J. **549**, 93 (2001)
 - [50] S. Inagaki, D. Lynden-Bell, Mon. not. R. astron. Soc. **205**, 913 (1983)
 - [51] E. Bettwieser, D. Sugimoto, Mon. not. R. astron. Soc. **208**, 493 (1984)
 - [52] P.H. Chavanis, M. Ribot, C. Rosier, C. Sire, Banach Center Publ. **66**, 103 (2004)
 - [53] P.H. Chavanis, Physica A **340**, 57 (2004); Physica A **387**, 5716 (2008)
 - [54] P.H. Chavanis, R. Mannella, Eur. Phys. J. B **78**, 139 (2010)
 - [55] P.H. Chavanis, C. Sire, Phys. Rev. E **73**, 066103 (2006)
 - [56] U.M.B. Marconi, P. Tarazona, J. Chem. Phys. **110**, 8032 (1999)
 - [57] J. Messer, H. Spohn, J. Stat. Phys. **29**, 561 (1982)
 - [58] R. Evans, Adv. Phys. **28**, 143 (1979)
 - [59] J. P. Hansen, I. R. MacDonald, *Theory of Simple Liquids* (Academic, London, 1986)
 - [60] P.H. Chavanis, A&A **432**, 117 (2005)
 - [61] We can obtain a larger class of models (see [3] and Appendix A) by letting the friction coefficient ξ depend on the density, $\xi = \xi(\rho)$, or more generally be a function of position and time, $\xi = \xi(\mathbf{r}, t)$.
 - [62] To avoid misunderstandings, we stress that the Smoluchowski-Poisson system does *not* describe traditional astrophysical systems. Indeed, astrophysical systems are not in a strong friction limit but rather in a weak (or no) friction limit. For example, stars are described by

the Euler-Poisson system (hydrodynamics) [21], galaxies by the Vlasov-Poisson system (collisionless dynamics) [22] and globular clusters by the Vlasov-Landau-Poisson system (collisional dynamics) [23]. The Smoluchowski-Poisson system could describe the dynamics of dust particles in the protoplanetary nebula, where particles experience a friction with the gas and a stochastic force due to turbulence or other diffusive effects [24]. Unfortunately, when the dust particles are small, the friction force is strong but the gravitational interaction is weak. Alternatively, when the particles are large, the gravitational interaction is strong but the friction force is weak. Therefore, the Smoluchowski-Poisson system is only valid in an intermediate regime which may not be the most relevant. Nevertheless, in the context of the statistical mechanics of self-gravitating systems [25, 26], the model of self-gravitating Brownian particles is interesting at a conceptual level because it provides a dynamical model associated with the *canonical ensemble* [1] while stellar systems are associated with the *microcanonical ensemble* [27, 28]. It can be used therefore to illustrate the notion of ensemble inequivalence that is generic for systems with long-range interactions [6].

[63] The theoretical interest of these equations was stressed early in [2] before all their possible applications were re-

alized.

[64] The case of repulsive interactions $G < 0$ is treated in Appendix E.

[65] Note that the dimension $d = 2$ is particularly relevant in chemotaxis [29] and for the dynamics of colloids at fluid interface [30].

[66] The excess free energy $F_{ex}[\rho]$ is a non-trivial functional determined by the short-range interactions. All the difficulty in the theory of fluids is to find some approximate forms of this functional. Once this functional is determined, the density profile, as well as all the n -point correlation functions, can be obtained via functional differentiation. Inversely, the excess free energy is often obtained from the study of the correlation functions. The excess free energy F_{ex} is known exactly only in a few particular cases, but very good approximations can be devised in more general cases [58, 59].

[67] This is not always the case. For example, the free energy associated with the Smoluchowski-Poisson system describing self-gravitating Brownian particles is not bounded from below [36, 37, 44, 45]. In that case, the system can experience an isothermal collapse. However, there also exists long-lived metastable states on which the system can settle [36, 45, 60].